PCCP

ROYAL SOCIETY OF CHEMISTRY

PAPER

View Article Online
View Journal | View Issue

Cite this: *Phys. Chem. Chem. Phys.*, 2025, **27**, 25980

Prediction of electronic, magnetic, and structural stability characteristics in Al- and Ga-doped single-walled SiC nanotubes: *ab initio* study using DFT

Vusala Nabi Jafarova, *[a] Raida Zabit Ibaeva,[bc] Sevda Rzayeva,[a] Khayala Ajdar Hasanova,[ab] M. E. Aliyev,[d] Ionut Cristian Scurtu,[e] Adrian Popa[e] and Octavian Narcis Volintiru[e]

We investigate the effects of Al- and Ga-defects on the electronic, magnetic, and structural stability of single-walled (6,0) SiC nanotubes (SWSiCNTs) through density functional theory simulations. Our results show that doping at either Si or C sites dramatically alters electronic behavior: Al doping at the Si site yields half-metallic behavior at 8.3% concentration (spin-up band gap ∼1.40 eV; spin-down channel metallic), while double doping (16.6%) yields full metallicity in both spin channels. Ga doping at the Si site shows semiconducting gaps for both spins at lower doping (8.3%), but transitions toward half-metallicity at higher doping (16.6%) with the spin-down channel becoming metallic. Doping at the C site preserves semiconducting behavior in both spin channels but introduces strong spin asymmetry: *e.g.* for Al doping at C, band gaps drop to ∼0.66 eV (spin-up) and ∼0.51 eV (spin-down) at 8.3%; for Ga at C, gaps reduce to ∼0.44 eV/0.60 eV at 8.3% and ∼0.26 eV at 16.6% for both spins. Partial density of states (PDOS) analyses reveal that near-Fermi states are dominated by carbon p orbitals and dopant d orbitals. Magnetic moment calculations show total magnetic moments around 1.0μ_B for single dopants, with much larger moments (∼8.5μ_B) for double Al dopants at C sites, and ∼6.0μ_B for double Ga at C. Both Al- and Ga-doped SWSiCNTs prefer antiferromagnetic ground states when substituted at Si sites, whereas Ga doping at C sites favors a ferromagnetic configuration. Stability assessments including geometry optimization, stress tensor and force analysis, and *ab initio* molecular dynamics demonstrate that all studied configurations are thermodynamically stable; however, Al-doped tubes generally show superior kinetic and mechanical stability, with lower residual forces, smaller stress tensor norms, and more modest thermal fluctuations during AIMD. Phonon band structure calculations further confirm the dynamical stability of all Al- and Ga-doped (6,0) SiCNT systems, as no imaginary frequencies were observed across the Brillouin zone, verifying that the optimized configurations are mechanically and vibrationally stable. These findings suggest that tuned doping (type, site, concentration) in SiC nanotubes can achieve desirable half-metallicity and robust magnetic behavior, positioning Al- and Ga-doped (6,0) SWSiCNTs as strong candidates for spintronic applications.

Received 12th September 2025,
Accepted 10th November 2025

DOI: 10.1039/d5cp03523f

rsc.li/pccp

1. Introduction

Graphene-like semiconductor materials have recently attracted significant research attention for applications in spintronics and optoelectronics due to their unique physical and chemical properties.[1–3] Among them, silicon carbide (SiC), as a third-generation wide-bandgap semiconductor, has been widely utilized in high-voltage, high-temperature, high-frequency, and high-power devices owing to its large band gap, excellent thermal conductivity, chemical stability, and mechanical robustness. Additionally, SiC has found roles in biocompatibility research, biomedical sensing, and energy harvesting applications.[1–9]

Theoretical and experimental studies have revealed that silicon carbide nanotubes (SiCNTs) possess more stable electronic and magnetic properties compared to carbon nanotubes

[a] *Azerbaijan State Oil and Industry University, 20 Azalig Ave., AZ-1010, Baku, Azerbaijan. E-mail: vusala.cafarova@asoiu.edu.az*
[b] *Ministry of Science and Education Republic of Azerbaijan, Institute of Physics, 131 H. Javid Ave., AZ-1143 Baku, Azerbaijan*
[c] *Baku State University, AZ 1148, Baku, Azerbaijan*
[d] *Nakhchivan State University, Nakhchivan, Azerbaijan*
[e] *Mircea cel Batran Naval Academy, Str. Fulgerului, nr.1, 900218 Constanta, Romania*

(CNTs).[2–6] In efforts to expand the applicability of 1D, 2D, and 3D Si-based nanomaterials, researchers have focused on doping with various impurity atoms to tailor their physical properties. Metal- and transition-metal-doped single-walled SiCNTs (SWSiCNTs) have shown significant potential for use in chemical sensors, hydrogen storage, and nanoscale spintronic devices. The introduction of dopants leads to charge redistribution and can induce magnetic behavior near the SiCNT framework. This ferromagnetic (FM) behavior typically arises due to hybridization involving the dopants' d orbitals.[10,11]

Previous studies using density functional theory (DFT) have demonstrated the feasibility of tuning the electronic and magnetic properties of SiCNTs through doping. For example, Zhang *et al.*[1] investigated Fe-doped SiCNTs and observed that the system exhibits half-metallic antiferromagnetic (AFM) or FM behavior depending on the dopant site. Similarly, the adsorption behavior of a series of transition metals (TMs) on SWSiCNTs was explored, revealing strong chemical binding with energies ranging from 1.17 eV to 3.18 eV for Cu to Pt atoms.[12] Heidarzadeh[13] found that Co doping induced a metallic nature in cubic SiC, while Mn- and Fe-doped (8,0) SiCNTs were reported to show half-metallicity – making them suitable for spintronic applications.[14] Other DFT-based studies have addressed the electronic and optical properties of various SiCNT chiralities, confirming their indirect bandgap semiconducting nature.[15,16]

Silicon and carbon, sharing similar valence electron configurations, have long been theorized to form fullerene-like and nanotube structures, including the chiral (6,0) SWSiCNTs.[17] More recently, extensive first-principles studies, including those combining DFT with machine learning, have uncovered the potential of noble-metal-doped SiC nanotubes (*e.g.*, Ag and Au) to exhibit tunable magnetic characteristics desirable for spintronic device integration.[18–20] These advanced computational approaches have also enabled accurate predictions of electronic density of states and magnetic transitions under various doping conditions.[21] In particular, transition-metal dopants such as V and Co have demonstrated robust ferromagnetic behavior and elevated Curie temperatures in SiCNTs, further highlighting their viability for magnetic applications.[20,22–24]

Recent theoretical investigations have explored the effects of group-III element doping in SiC nanotubes, such as the study by Wu *et al.*,[25] who used first-principles calculations to examine Al and P doping in (6,0) SiC nanotubes and found that Al substitution significantly modulates electronic properties, suggesting tunable semiconducting behavior. In a related context, Peyghan *et al.*[26] conducted a DFT study on Al- and Ga-doped single-walled boron nitride nanotubes, demonstrating enhanced adsorption energy for CO molecules due to doping, thereby highlighting the chemical sensitivity induced by group-III elements. Doust Mohammadi *et al.*[27] investigated the adsorption behavior of H_2SiCl_2 on Al- and Ga-doped boron nitride nanotubes and found that these dopants significantly improved surface reactivity, which may be extended to similar behavior in SiC-based systems. Hamad and Al-Douri[28] used DFT to analyze the interactions of doped carbon nanotubes (including Al doping) with sulfur-containing gases, concluding that Al doping improves adsorption and sensing performance, thereby confirming the functional impact of p-block dopants on nanotube surfaces.

The motivation behind this research lies in the need to discover and design novel spintronic materials with tunable magnetic properties, where doping SiC nanotubes with group-III elements like Al and Ga offers a promising route. Understanding how such dopants influence the electronic and magnetic behavior of SiCNTs can enable the development of next-generation nanoscale devices with enhanced performance and stability. Studying Al- and Ga-doped SWSiCNT systems is important because group-III elements introduce distinct electronic and magnetic modifications compared to transition metals, potentially leading to stable, lightweight, and non-toxic spintronic materials. While most prior research has focused on transition metal dopants, the investigation of p-block dopants like Al and Ga remains largely unexplored. This work provides novel insight into how such dopants influence the spin polarization and magnetic moment distribution in (6,0) SiCNTs, offering a new avenue for designing non-magnetic-element-based spintronic nanodevices. The exploration of Al- and Ga-doped SiC nanotubes is crucial due to their potential to introduce unique electronic and magnetic properties distinct from those of transition metal-doped systems. These group-III elements can modify the electronic structure of SiCNTs, offering new avenues for designing materials with tailored properties for spintronic and optoelectronic applications.

Doped nanotubes can stabilize isolated metal atoms, acting as active sites for single-atom catalysis (SAC), offering high catalytic efficiency and selectivity. Although direct SAC studies on Al- or Ga-doped SiC nanotubes are limited, similar behavior has been observed in doped graphene and other defective two-dimensional materials, suggesting that such doping strategies may enable catalytic functionalities in SiCNTs as well.[29] Additionally, Al- and Ga-doped boron nitride nanotubes and related nanostructures have demonstrated enhanced adsorption capabilities for toxic gases such as H_2SiCl_2, H_2S, and SO_2, indicating the potential of doped SiCNTs for use in gas sensing technologies.[30–32] In the field of nanoelectronics, first-principles studies have shown that doping SiC nanotubes with elements like Al and P can modulate their electronic band structure and defect formation energies, making them suitable candidates for nanoscale electronic and optoelectronic devices.[33] Furthermore, if doping induces magnetic moments in these systems, the resulting spin polarization may be harnessed in spintronic devices, where control of electron spin is essential for data storage and logic applications.[34] Finally, due to their chemical stability, high surface area, and tunable surface reactivity, doped SiC-based nanostructures are also being explored for energy-related applications, including hydrogen storage, photocatalysis, and use as electrode materials in energy conversion and storage devices.[33,35]

The limited existing studies on Al- and Ga-doped SiCNTs highlight the novelty of this research, aiming to fill this gap and

expand the understanding of doping effects in SiC-based nanomaterials. In this study, we present a comprehensive first-principles investigation of the electronic and magnetic properties of Al- and Ga-doped single-walled SiCNTs with (6,0) chirality. By analyzing the spin-polarized electronic structures, total and partial density of states (DOS), and evaluating both total and local magnetic moments, we aim to elucidate how these group-III dopants influence the magnetic characteristics of the system. Our findings provide new insight into the design of Si-based nanostructures for use in future spintronic devices.

2. Computational details

In this study, first-principles calculations were performed using the Atomistix ToolKit (ATK) (ATK V-2023.09, **https://quantumwise.com/**) simulation package to investigate the electronic and magnetic properties of Al- and Ga-doped single-walled silicon carbide nanotube (SWSiCNT) systems, each consisting of 24 atoms in the unit cell. The calculations were conducted within the framework of density functional theory (DFT),[36] employing the local spin density approximation (LSDA)[37] for the exchange–correlation potential and utilizing FHI-type pseudopotentials[38] to describe the electron–ion interactions.

DFT is a quantum mechanical modeling method used to analyze the electronic structure of many-body systems, such as atoms, molecules, and solids. Instead of solving the full many-body Schrödinger equation, DFT simplifies the problem by focusing on the electron density $\rho(r)$ as the central quantity. The foundational equations in DFT are the Kohn–Sham equations, which are derived by minimizing the total energy functional with respect to the electron density.

In spin-polarized DFT, LSDA is a foundational yet effective approach for describing magnetic phenomena. It accounts for spin-dependent electron density, which is essential for accurately modeling systems with unpaired electrons, local magnetic moments, and magnetic ordering. Within the LSDA formalism, the total electron density is separated into spin-up ($\rho^{\uparrow}$) and spin-down ($\rho^{\downarrow}$) components. The total spin magnetization M of the system is then defined as:

$$M = \int \left[\rho^{\uparrow}(r) - \rho^{\downarrow}(r)\right] \mathrm{d}r \tag{1}$$

It is well known that standard implementations of DFT often underestimate the band gap of semiconductors. To address this limitation, the DFT+U method-specifically the local spin density approximation with Hubbard U (LSDA+U)[39] introduces an on-site Coulomb interaction term that improves the description of localized electrons. This correction is particularly important in systems where LSDA fails due to self-interaction errors. The selection of a suitable computational approach has largely mitigated this issue for many materials.

Recent advances in simulation techniques, particularly the incorporation of semi-empirical Hubbard U corrections,[39] have enabled more accurate theoretical predictions of semiconductor band gaps. In this work, the Hubbard U parameter is implemented using simplified schemes described in ref. 40 and 41.

In our spin-polarized DFT calculations, both the Hamiltonian and the density matrices were explicitly extended to incorporate spin degrees of freedom, thereby enabling independent treatment of spin-up and spin-down electron channels. This formalism allows for a detailed and accurate analysis of magnetic properties and spin asymmetries in the electronic structure. Throughout the calculations, we adopted a collinear spin approximation, wherein all magnetic moments are constrained to align either parallel or antiparallel. This assumption is commonly employed in systems where non-collinear magnetic effects are negligible, such as those involving localized 3d transition-metal dopants in SiC nanotubes.

The LSDA was chosen as the exchange–correlation functional due to its computational efficiency and its proven capability to capture spin polarization effects in transition-metal-doped semiconductors, as demonstrated in previous studies. Additionally, spin-resolved density of states (DOS) and magnetic moments were analyzed using Mulliken population analysis,[42] providing deeper insight into the spatial distribution and origin of magnetization within the system. Furthermore, the spin density distribution was analyzed to evaluate the contributions of individual atoms to the overall magnetic behavior. This was accomplished by examining the spatial distribution of the spin difference density, $\rho^{\uparrow}-\rho^{\downarrow}$, which provides a clear depiction of spin localization and magnetic interactions in the vicinity of the dopant atoms.

Mulliken population analysis[42] was employed to compute the magnetic moments of 3d transition metal-doped SWSiCNTs. As a classical method in quantum chemistry, Mulliken analysis provides insight into the distribution of electrons within a molecule by partitioning the total electron density among atoms and their respective orbitals. This method is grounded in the results of DFT calculations and utilizes molecular orbitals (MOs) and basis functions to estimate atomic charges, orbital contributions, and bond populations. Mulliken population analysis[42] is particularly valuable for understanding the magnetic properties of molecular and extended systems, especially those containing unpaired electrons. In spin-polarized DFT calculations, the electron density is separated into α-spin (spin-up) and β-spin (spin-down) components. Mulliken analysis facilitates the evaluation of spin-resolved electron populations on each atom. In the present study, the spin-resolved Mulliken populations were extracted from spin-polarized DFT calculations to determine the local magnetic moments of individual atoms. Specifically, the local spin magnetic moment of each atom was computed as the difference between its Mulliken α-spin and β-spin electron populations. The local magnetic moment on a given atom A is calculated as the difference between its Mulliken α- and β-spin populations:

$$\mu^{\mathrm{A}} = N_{\alpha}^{\mathrm{A}} - N_{\beta}^{\mathrm{A}} \tag{2}$$

where N_{α}^{A} and N_{β}^{A} are the numbers of α-spin and β-spin electrons, respectively, assigned to atom A. A nonzero value of μ^{A} indicates the presence of a local magnetic moment on that

atom. The sign and magnitude of this moment provide insights into the magnetic ordering and coupling behavior of the system. This allowed us to identify and quantify the magnetic contributions of the TM dopant atoms as well as their neighboring Si and C atoms in the nanotube structure. The obtained local spin magnetic moments are presented and discussed in detail in Sections 3.5–3.8, with numerical results provided in Tables 5–8.

For TM-doped SWSiCNTs, the partially filled 3d orbitals of the transition metal atoms introduce localized unpaired electrons, which often result in significant magnetic moments. Mulliken population analysis helps to identify not only the magnitude of these moments but also how they are distributed across the M atom and nearby Si and C atoms in the nanotube framework. This information is essential for understanding the magnetic behavior of doped nanostructures and their potential applications in spintronics or magnetic sensing devices.

Mulliken population analysis was performed to obtain the occupation number of each atomic orbital. The magnetic moments were then calculated as the difference between the spin-up and spin-down electron populations. The partial density of states (PDOS) for each spin channel was obtained by expanding the discrete energy levels using the Lorentzian broadening function,[43] where the energy levels correspond to the one-electron eigenvalues. The integral of the PDOS $D^{\alpha}_{nl\sigma}(E)$ over an energy interval E_1 to E_2 yields the number of one-electron states within that range. Typically, the δ-functions representing discrete energy levels are broadened using Lorentzian functions to make graphical representation possible:

$$D^{\alpha}_{nl\sigma}(E) = \sum_i A^{\alpha}_{nl\sigma i} \frac{\delta/\pi}{(E-\varepsilon_{i\sigma})^2+\delta^2}, \quad (3)$$

where $\varepsilon_{i\sigma}$ denote the one-electron energies, i is index of the energy level, and σ represents the spin state, and $A^{\alpha}_{nl\sigma i}$ refers to the atomic orbital on atom α.

The total DOS is obtained by summing the PDOS contributions for atom α at energy E, which includes a summation over all its orbitals characterized by quantum numbers (n, l) and and spin states (σ), and is typically expressed as eqn (4)

$$D_{\sigma}(E) = \sum_{nl\alpha} D^{\alpha}_{nl\sigma}(E). \quad (4)$$

The quantum-confined SWSiCNT with a chiral vector of (6,0) was theoretically designed using DFT calculations. Magnetic dopants, specifically Al and Ga, were introduced as substitutional atoms in the SiC SWNT to investigate their impact on the electronic and magnetic properties of the system. The calculations were carried out using the LSDA along with Hubbard U corrections[39] to better describe on-site Coulomb interactions in localized orbitals. In this study, semi-empirical Hubbard U parameters were applied to improve the accuracy of the predicted electronic structure. Specifically, a U_d value of 5 eV was applied to the d-orbitals of silicon atoms, and a U_p value of 4.8 eV was applied to the p-orbitals of carbon atoms, in order to more accurately reproduce the energy gap of the system. The applied Hubbard U values for individual atoms are as follows: Si1, Si2, Si3,. . .: U_d = 5 eV; C1, C2, C3,. . .: U_p = 4.8 eV.

Special k-point sampling was performed using a Monkhorst–Pack grid of 1 × 1 × 5 k-points[44] to ensure accurate Brillouin zone integration. This grid provides dense sampling along the periodic z-axis, which corresponds to the longitudinal direction of the nanotube. The plane-wave kinetic energy cutoff was set to 100 Ry (equivalent to 50 Hartree), and all structures were fully relaxed through geometry optimization at an electron temperature of 300 K. The convergence criteria for atomic forces and cell stress were set to be less than 0.001 eV Å^{-1} and 0.001 eV Å^{-3}, respectively. Valence electron configurations used in the calculations were as follows: silicon (4 valence electrons: [Ne] $3s^2 3p^2$), carbon (4 valence electrons: [He] $2s^2 2p^2$), aluminum (3 valence electrons: [Ne] $3s^2 3p^1$), and gallium (3 valence electrons: [Ar] $4s^2 4p^1$).

This study investigates the effect of doping concentration on the electronic and magnetic properties of silicon carbide nanotubes (SiCNTs). We consider substitutional doping of aluminum (Al) and gallium (Ga) atoms at both silicon (Si) and carbon (C) sites. Specifically, single doping with Al or Ga at an 8.3% concentration and double (co-) doping with both Al and Ga at a 16.6% concentration are analyzed. By comparing these doping strategies, we aim to understand how different dopant types, substitutional sites, and concentrations influence the fundamental properties of SiCNTs. This knowledge is crucial for optimizing their performance in nanoelectronic and spintronic applications. To investigate the ferromagnetic (FM) and antiferromagnetic (AFM) behaviors of diluted magnetic SiC nanotubes, silicon (Si) and carbon (C) atoms were partially substituted by magnetic dopants Al/Ga. For the FM configuration, the dopants were aligned with parallel spins Al/Ga$^{\uparrow}{}_{x/2}$; Al/Ga$^{\uparrow}{}_{x/2}$, while for the AFM configuration, the dopants had antiparallel spins Al/Ga$^{\uparrow}{}_{x/2}$; Al/Ga$^{\downarrow}{}_{x/2}$. Here, the arrows ↑ and ↓ denote the orientation of the local magnetic moments of the metal dopants.

In addition to the electronic and magnetic analyses, the thermodynamic, kinetic, and mechanical stability of the pristine and doped SWSiCNTs were examined through total energy, atomic force, and stress tensor evaluations, followed by *ab initio* molecular dynamics (AIMD) simulations to confirm thermal robustness. Furthermore, to verify the dynamical stability of the Al- and Ga-doped SWSiCNT systems at Si and C sites, phonon dispersion relations were calculated using the finite-displacement method as implemented in the Quantum ATK package. Geometry-optimized structures obtained within the spin-polarized DFT-LSDA framework (Perdew–Zunger parametrization) and FHI norm-conserving pseudopotentials were used as the input configurations. For each optimized model, small atomic displacements of 0.01 Å were introduced to construct the dynamical matrix, with the acoustic sum rule (ASR) enforced to eliminate spurious imaginary modes.

The phonon band structures were computed along the high-symmetry path Γ–Z with 50–120 k-points per segment. The absence of imaginary frequencies in all configurations confirms the dynamical stability and validates the experimental

synthesizability of the Al- and Ga-doped SiCNTs. The calculations were performed using a real-space mesh cutoff of 100 Hartree, a Monkhorst–Pack k-grid of $1 \times 1 \times 10$, and the finite-difference central scheme for force constant evaluation.

3. Results and discussion

3.1. Electronic structure for $Al_xSi_{1-x}C$ NT

In this section, we explore the effects of aluminum (Al) doping at the Si site on the electronic structure of (6,0) SWSiCNTs through DFT calculations. In addition to electronic structure analysis, Bader charge analysis was performed to investigate charge redistribution caused by the Al substitution.

The pristine SiC nanotube has a characteristic bond length of 1.88 Å between silicon and carbon atoms, and a radius of approximately 3.11 Å, defining its structural stability and nanoscale geometry. The doping of Al atoms into the SiC nanotube lattice introduces significant modifications to its electronic properties, especially its spin-dependent behavior. Using spin-polarized DFT within the LSDA framework, we calculated the spin-resolved band structures and densities of states (DOS) for the $Al_xSi_{1-x}C$ NT. The electronic band structure is split into two spin channels due to the presence of unpaired electrons associated with the magnetic dopant.

For comparison, the undoped bulk SiC material shows an underestimated band gap within LSDA (3.8 eV direct, 2.1 eV indirect) relative to the experimental gap ($\sim$3.33 eV).[45] This discrepancy is a common shortcoming of standard DFT approaches due to their approximate treatment of electron–electron interactions. To improve accuracy, Hubbard U corrections were applied, specifically targeting the localized 3d orbitals of silicon and 2p orbitals of carbon, which are critical for correctly modeling correlation effects in these states. With Hubbard U included (DFT-LSDA+U), the band gaps were corrected upward to 5.2 eV (direct) and 3.3 eV (indirect), matching well with experimental[45] and previous theoretical values.[46] This confirms the system's semiconducting nature and validates the computational approach. It should be noted that we obtained a band gap of 0.98 eV for the undoped single-walled SiC nanotube (SWSiCNT) from first-principles calculations, and this result, along with the computational details, was published in our previous work.[21]

When aluminum is introduced as a dopant in the SiC nanotube (Fig. 1), it replaces silicon atoms and contributes additional electronic states near the Fermi level. This asymmetric electronic structure between spins is characteristic of a half-metal, where one spin channel is metallic (conducting) and the other is semiconducting. This half-metallic behavior is highly desirable for spintronic applications, as it allows for 100% spin-polarized currents, enabling devices that exploit electron spin rather than charge for information processing and storage.

To explore the influence of doping concentration on the electronic and magnetic properties of SiCNTs, this study investigates the effects of two different doping levels 8.3% (for single doped) and 16.6% (for double doped) using aluminum (Al) atom at the Si site. Understanding how varying dopant concentrations alter the fundamental properties of SiCNTs is of considerable research interest, as it provides valuable insights for tuning the material's behavior for potential applications in nanoelectronics and spintronics. For the case of 8.3% Al doping at the Si site in the SiC nanotube, our spin-polarized band structure results reveal a distinct spin splitting: the majority-spin channel exhibits a band gap of 1.4 eV, while the minority-spin channel becomes metallic, with its band gap closing to zero. Additionally, when two aluminum (Al) atoms are doped at two silicon (Si) sites in the SWSiCNT, both the spin-up and spin-down bands cross the Fermi level, indicating a metallic nature.

The partial density of states (PDOS) analysis reveals that the states near the Fermi level predominantly originate from the p orbitals of carbon atoms and the d orbitals of aluminum dopants. This hybridization influences the magnetic moment

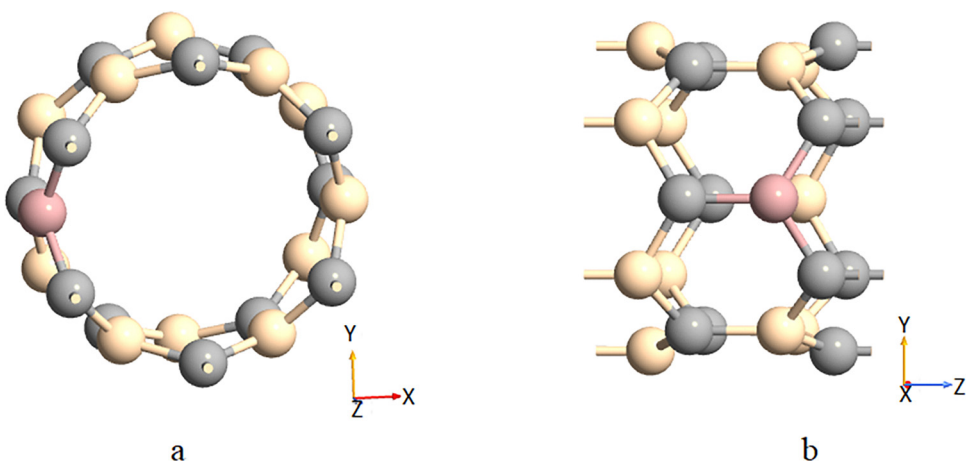

Fig. 1 The top (a) and side (b) views of Al/Ga-doped at Si site in (6,0) SWSiCNT structures. The gray, beige, and pink balls represent carbon, silicon, and impurity (Al/Ga) atom, respectively.

localization and electronic transport properties. The calculated band structures, total and partial density of states (DOS) diagrams for $Al_xSi_{1-x}C$ NT, are presented in Fig. 2 and 3, respectively.

In the case of the Al-doped SiC nanotube system, the spin-down band gap is significantly reduced to 0 eV, resulting in metallic behavior due to the crossing of the Fermi energy level near the Γ point of the Brillouin zone. This closure of the spin-down gap leads to an increased density of states around the Fermi level, which in turn enhances the electrical conductivity of the Al-doped SiC nanotube.

Our calculations reveal that the electronic states at the Fermi level have a significant contribution from the aluminum 4d orbitals, indicating a moderate orbital overlap between the carbon 2p orbitals and the aluminum 4d orbitals. This orbital interaction plays an important role in modifying the electronic structure and magnetic properties of the system, facilitating the transition to a half-metallic state with spin-polarized conduction.

Table 1 summarizes the calculated band gap values and electronic characteristics of undoped and Al-doped bulk SiC and SWSiCNTs under different doping conditions. The undoped bulk SiC, with Hubbard U correction, shows a band gap consistent with experimental[45] and theoretical results,[46] confirming the reliability of the computational approach. The undoped SWSiCNT, with a band gap of 0.98 eV, serves as a reference and is taken from our previous work.[21]

When aluminum is introduced as a dopant at 8.3%, the system exhibits half-metallic behavior due to spin asymmetry in the band structure. At a higher doping level of 16.6%, the nanotube becomes fully metallic, with both spin channels crossing the Fermi level. This progression clearly illustrates how doping concentration influences the electronic nature of SiCNTs, which is critical for designing materials with tailored properties for spintronic and nanoelectronic applications. The calculated band structures and total density of states (TDOS) diagram for the double Al-doped SWSiCNT system at the Si site are provided in SI1.

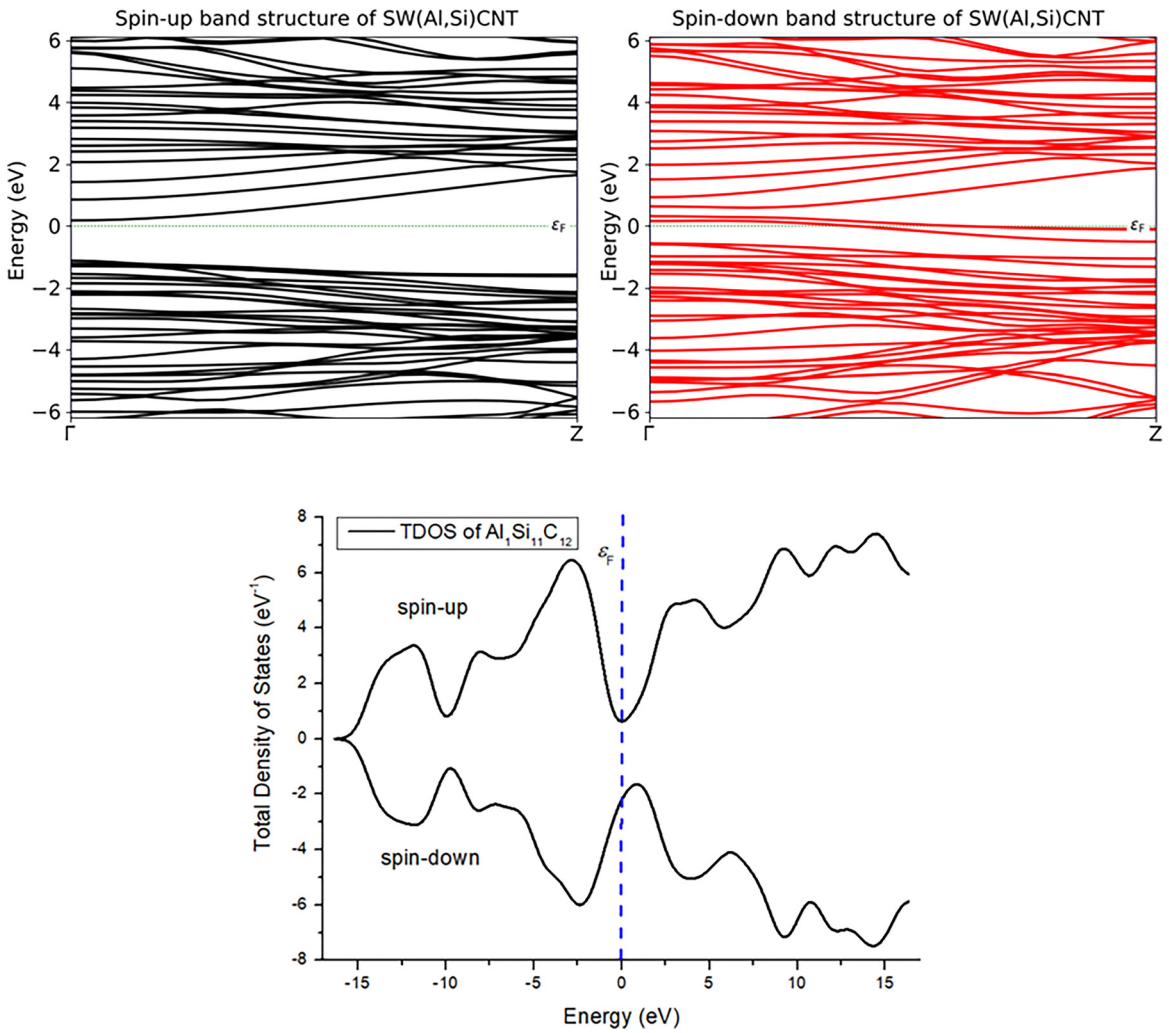

Fig. 2 The calculated spin-up (black) and spin-down (red) band structures and TDOS diagram for $Al_xSi_{1-x}C$ NTs.

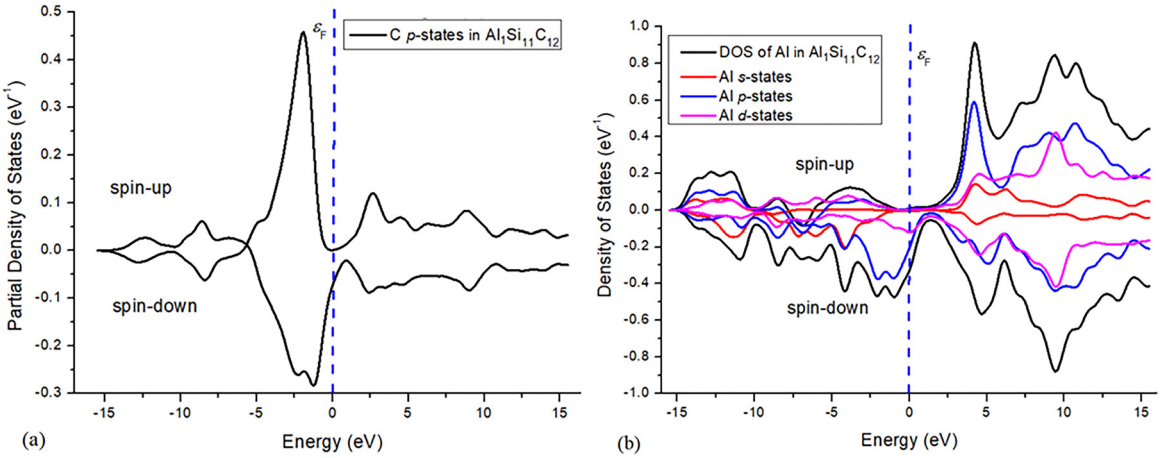

Fig. 3 The calculated PDOS from C (a), and Al (b) atoms for $Al_xSi_{1-x}C$ NTs. Positive and negative DOS values represent majority and minority spin states, respectively.

Table 1 Comparison of calculated band gap values and electronic nature of undoped and Al-doped bulk SiC and SWSiCNTs under different doping conditions

System	Doping level	Band gap (eV)	Electronic nature	Remarks
Bulk SiC (undoped)	—	5.2 (direct), 3.3 (indirect)	Semiconductor	In agreement: exp.;[45] theory[46]
SWSiCNT (undoped)	0%	0.98	Semiconductor	Reported in previous work[21]
SWSiCNT (Al-doped at Si site)	8.3%	1.4 (↑), 0 (↓)	Half-metal	Spin asymmetry: semiconducting for majority spin, metallic for minority
SWSiCNT (Al-doped at 2 Si sites)	16.6%	0 (↑), 0 (↓)	Metal	Both spin channels metallic

To further elucidate the electronic charge redistribution upon Al doping, we performed Bader charge analysis for the Al-doped SWSiCNT system at the Si site. The Bader results indicate that the substituted Al atom exhibits a total charge of approximately 10.76 $|e|$, suggesting a charge loss of $\sim$2.24 $|e|$ compared to its neutral valence state (13 valence electrons for Al). This significant electron donation confirms the donor behavior of the Al dopant in the nanotube lattice.

In contrast, the nearby carbon atoms, especially those adjacent to the Al site, display Bader charges in the range of 8.25–8.37 $|e|$, corresponding to a gain of $\sim$2.25–2.37 $|e|$ relative to the neutral carbon valence of 6 electrons. This indicates that the donated electrons from the Al atom are primarily accepted by the surrounding carbon atoms, enhancing the Al–C orbital interactions. The silicon atoms in the pristine structure typically show Bader charges around 11.65–11.72 $|e|$, reflecting a charge loss of $\sim$2.3–2.35 $|e|$, consistent with their +4 oxidation state in SiC. The Al dopant behaves similarly in terms of net electron donation, further reinforcing its substitutional compatibility at the Si site. A full table of atomic charges for the Al-doped SWSiCNT at Si site is provided in SI2.

In summary, aluminum doping introduces magnetism and converts the SiC nanotube from a nonmagnetic semiconductor into a spin-polarized half-metallic system. The Bader charge analysis further reveals significant charge transfer between aluminum dopants and the surrounding atoms, confirming strong electronic interactions that underpin the observed changes in electronic and magnetic behavior. This tunability of both charge distribution and spin polarization makes Al-doped SiC nanotubes highly promising candidates for future nanoscale spintronic applications.

3.2. Electronic properties of $Ga_xSi_{1-x}C$ NT

In this section, we present the calculated majority and minority spin band structures, total density of states (TDOS), and partial density of states (PDOS) for gallium (Ga)-doped silicon sites in SWSiCNTs. In addition to the electronic structure analysis, Bader charge analysis has also been performed to investigate the charge redistribution upon Ga doping. This section explores the influence of doping concentration on the electronic and magnetic properties of silicon carbide nanotubes (SiCNTs), focusing specifically on two different Ga doping levels: 8.3% and 16.6%. By examining single-doped configurations at these concentrations, we aim to provide a comprehensive understanding of how varying Ga doping levels affect the material's behavior. Gaining insight into how different doping concentrations modify the fundamental properties of SiCNTs is of considerable research interest, as it offers valuable guidance for tuning these materials for potential applications in nanoelectronics and spintronics.

Using first-principles calculations, we determined the spin-up and spin-down band gaps of these systems. The resulting band structures, TDOS and PDOS diagrams are shown in Fig. 4 and 5, respectively. Fig. 4 spin-resolved band structure of

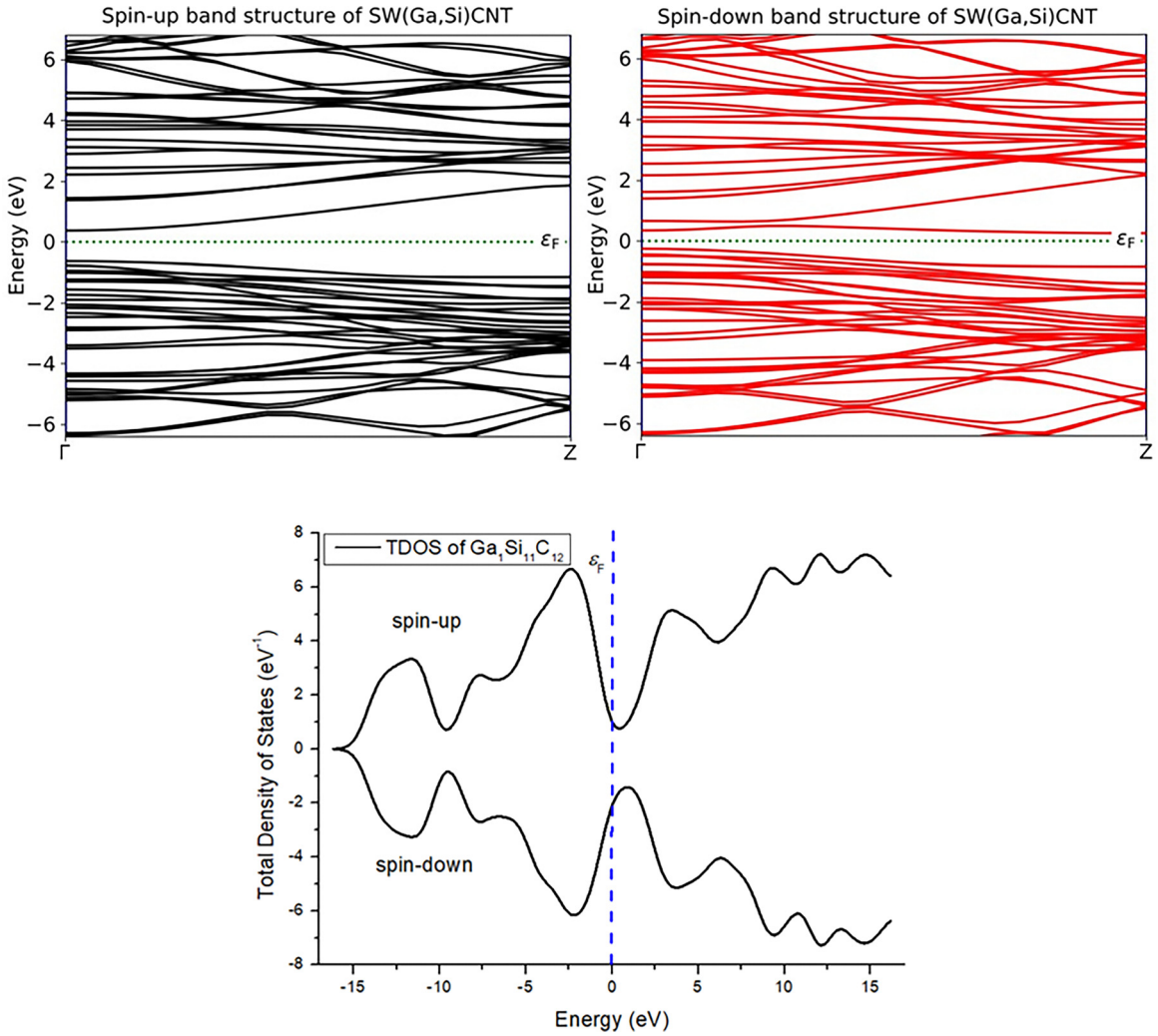

Fig. 4 The calculated spin-up (black) and spin-down (red) band structures, and TDOS diagram for $Ga_xSi_{1-x}C$ NTs.

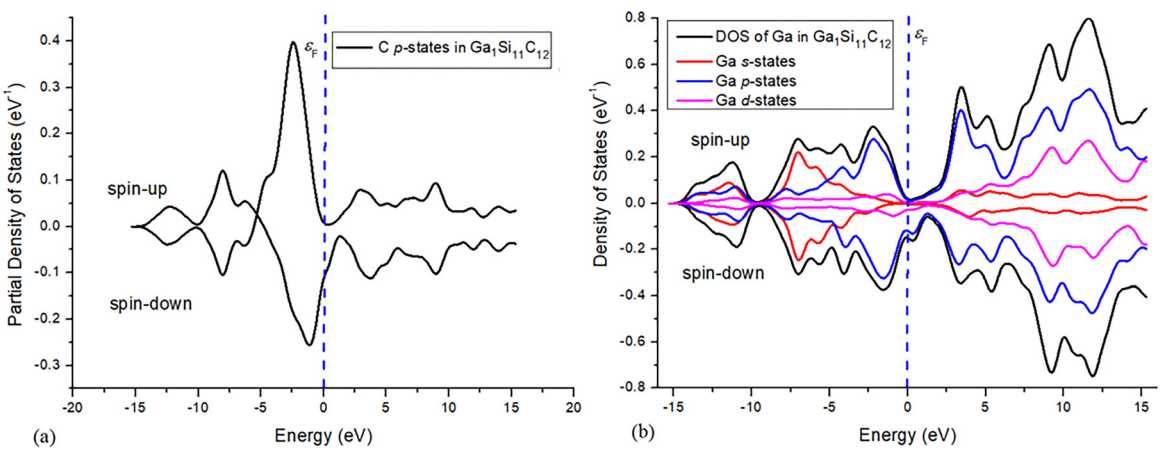

Fig. 5 Calculated PDOS for the C (a) and Ga (b) atoms in the $Ga_xSi_{1-x}C$ NTs. Positive and negative DOS values represent majority and minority spin states, respectively.

Ga-doped SWSiCNT system, showing semiconducting behavior in both spin-up and spin-down channels. From the band structure analysis of the single Ga-doped SWSiCNT with 8.3% doping concentration, where the Ga atom is substituted at the

Si site, we estimated the band gap widths to be approximately 1.0 eV for the majority spin states and 0.6 eV (direct) and 0.5 eV (indirect) for the minority spin states. For the double Ga-doped SWSiCNT, where two Ga atoms are substituted at Si sites (corresponding to a 16.6% doping level), the spin-up channel exhibits a band gap of approximately 1.2 eV, while the spin-down bands cross the Fermi level, resulting in a zero band gap. This spin asymmetry indicates a half-metallic nature, which is promising for spintronic applications. The calculated band structures and TDOS diagram for the double Ga-doped system at the Si site in SWSiCNT are provided in SI1.

First-principles simulations reveal that the minority spin band gap of the Ga-doped (6,0) SWSiCNT is significantly reduced to 0.5 eV, indicating that the system exhibits semiconducting behavior. Analysis of the partial density of states (PDOS) for the SiC:Ga nanotube shows that the electronic states near the Fermi level mainly originate from the p-orbitals of carbon and the d-orbitals of gallium. Specifically, the states at the Fermi energy have a notable contribution from the Ga 5d orbitals, indicating moderate orbital interaction between the C 2p and Ga 5d orbitals.

Table 2 presents the calculated spin-resolved band gaps of Ga-doped SWSiCNTs at different doping concentrations, along with their corresponding electronic characteristics. The undoped SWSiCNT exhibits a semiconducting nature with a band gap of 0.98 eV, as reported in our previous work.[21] At 8.3% Ga doping (single substitution at a Si site), the system shows a spin asymmetry, with a 1.0 eV gap for the spin-up channel and reduced band gaps of 0.6 eV (direct) and 0.5 eV (indirect) for the spin-down channel, indicating a semiconducting behavior. For the 16.6% Ga doping case (double substitution), the spin-up channel retains a semiconducting gap of 1.2 eV, while the spin-down bands cross the Fermi level, resulting in a zero band gap. This behavior confirms a robust half-metallic state, making Ga-doped SWSiCNTs promising candidates for spintronic applications due to their spin-selective conductivity.

To gain deeper insight into the electronic interactions within the Ga-doped SWSiCNT, where gallium replaces a silicon atom, we performed Bader charge analysis. The results indicate a noticeable difference in charge distribution compared to the Al-doped case. The Ga atom, doped at the Si site, exhibits a net Bader charge of approximately $-1.05e$, which is significantly less negative than that of the substituted Si atom ($-2.33e$). This implies that Ga donates fewer electrons to the surrounding lattice than Si, a behavior attributed to Ga's lower electronegativity and larger atomic radius. Nearby carbon atoms, especially C14 (positioned closest to the Ga site), gain a charge of about $+1.94e$, which is somewhat lower than the typical charge gain ($\sim+2.3e$) observed for C atoms near Si. This suggests a weaker covalent character in the Ga–C interaction compared to the original Si–C or Al–C bonds, potentially impacting the local electronic and magnetic properties.

In summary, the Bader charge analysis shows that Ga doping at the Si site leads to a reduced degree of charge transfer compared to Al doping. This reduced electron donation and weaker orbital interaction with neighboring C atoms are consistent with the relatively diminished spin polarization observed in the electronic structure. A full table of atomic charges for the Ga-doped SWSiCNT at Si site is provided in SI2.

3.3. Electronic properties of $SiC_{1-x}Al_x$ NT

In this section, we investigate the effects of aluminum (Al) doping at the carbon (C) site in the (6,0) SWSiCNT using spin-polarized density functional theory (DFT) calculations. While previous sections focused on Al substitution at the Si site, here the substitution is made at the C site to explore how the choice of doping site influences the electronic and magnetic properties of the system.

Fig. 6 displays the optimized atomic configurations of the Al/Ga-doped SWSiCNT, with top and side views illustrating the position of the Al dopant substituting a carbon atom. The structure remains geometrically stable, indicating the feasibility of doping at the C site. In these visualizations, gray, beige, and pink spheres represent C, Si, and dopant (Al/Ga) atoms, respectively.

The spin-resolved band structures and total density of states (TDOS) for the Al-doped system (at 8.3% concentration) are shown in Fig. 7. The spin-up channel exhibits a direct band gap of approximately 0.66 eV, while the spin-down channel shows a slightly smaller gap of 0.51 eV, indicating spin asymmetry in the electronic structure. Despite the reduction in band gaps compared to the undoped system, both spin channels retain semiconducting characteristics. To further investigate the effect of doping concentration, a second Al atom was introduced, replacing another carbon atom, resulting in a 16.6% doping level. This configuration enhances the interaction between dopant atoms and their surrounding lattice, significantly influencing the band structure. The spin-up channel retains a semiconducting gap of 0.60 eV, while the spin-down channel shows a much narrower gap of 0.12 eV. This marked disparity indicates stronger spin polarization and possible half-metallic tendencies depending on the Fermi level positioning and carrier concentration. The reduced spin-down gap suggests

Table 2 Calculated spin-up (↑) and spin-down (↓) band gaps of Ga-doped SWSiCNTs at different doping concentrations

System	Doping level	Band gap (eV)	Electronic Nature	Remarks
SWSiCNT (undoped)	0%	0.98	Semiconductor	Previous work[21]
SWSiCNT (Ga at Si site)	8.3%	1.0 (↑), 0.6 (direct) (↓), 0.5 (indirect) (↓)	Semiconductor	Spin asymmetry; majority spin semiconducting, minority spin nearly metallic
SWSiCNT (2 Ga at Si sites)	16.6%	1.2 (↑), 0 (↓)	Half-metal	Spin-down bands cross Fermi level

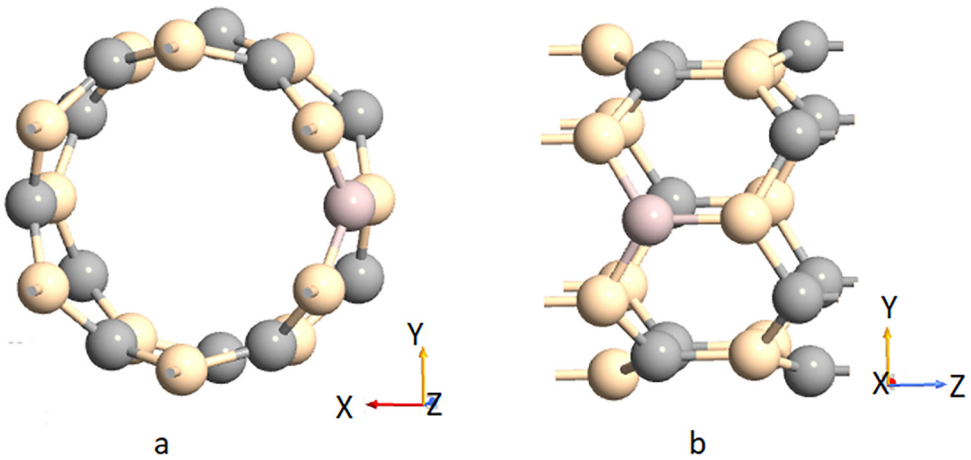

Fig. 6 The top (a) and side (b) views of Al-doped SWSiCNT at the C site. Gray: C atoms, beige: Si atoms, and pink: Al/Ga atom.

that the material could exhibit spin-dependent conductivity, a desirable trait in spintronic devices. The calculated band structures and TDOS diagram for the double Al-doped system at the C site in SWSiCNT are provided in SI1.

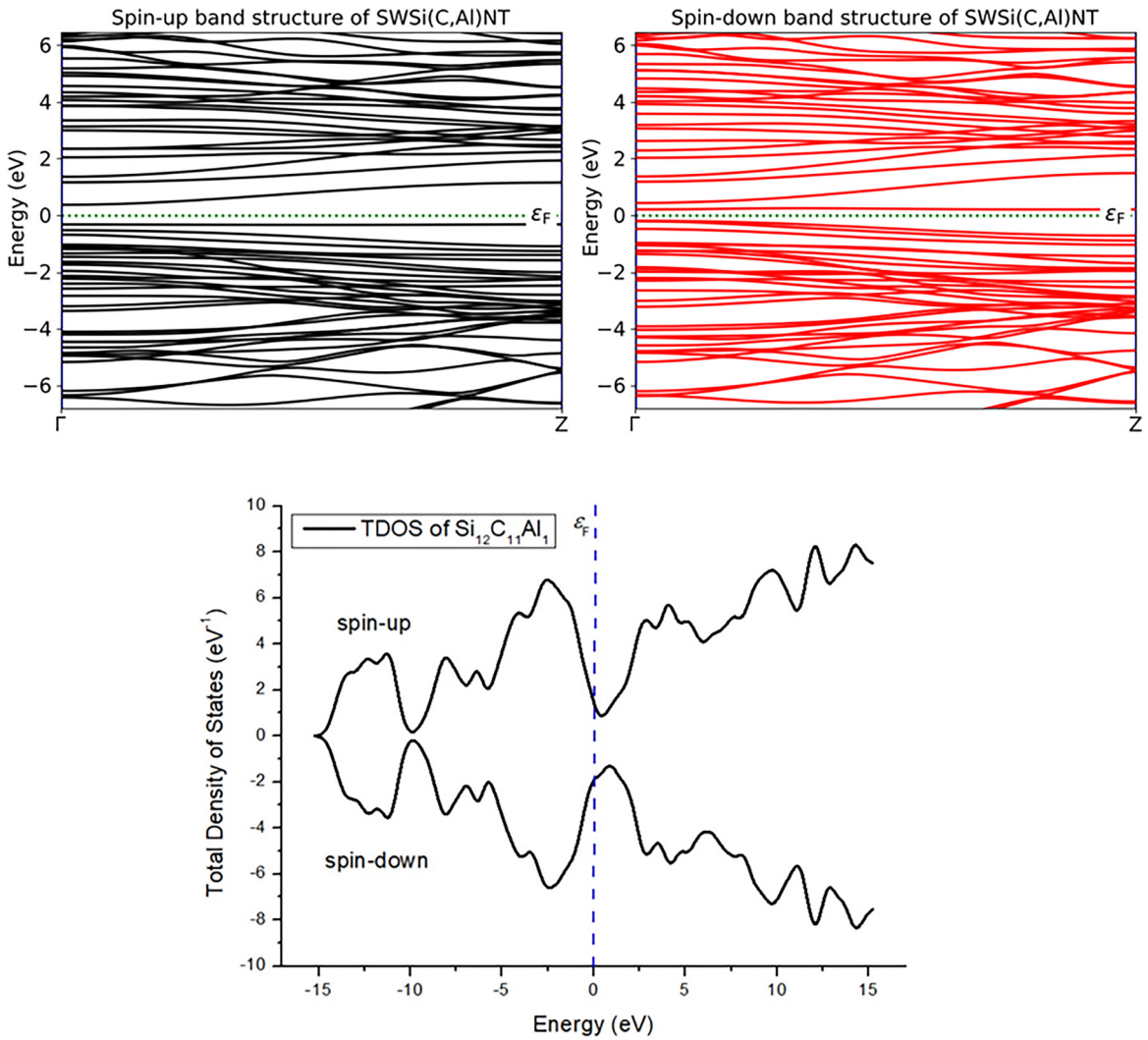

Fig. 7 Spin-up (black) and spin-down (red) band structures of $SiC_{1-x}Al_x$ NT, along with the TDOS. A spin asymmetry in the band gap is evident.

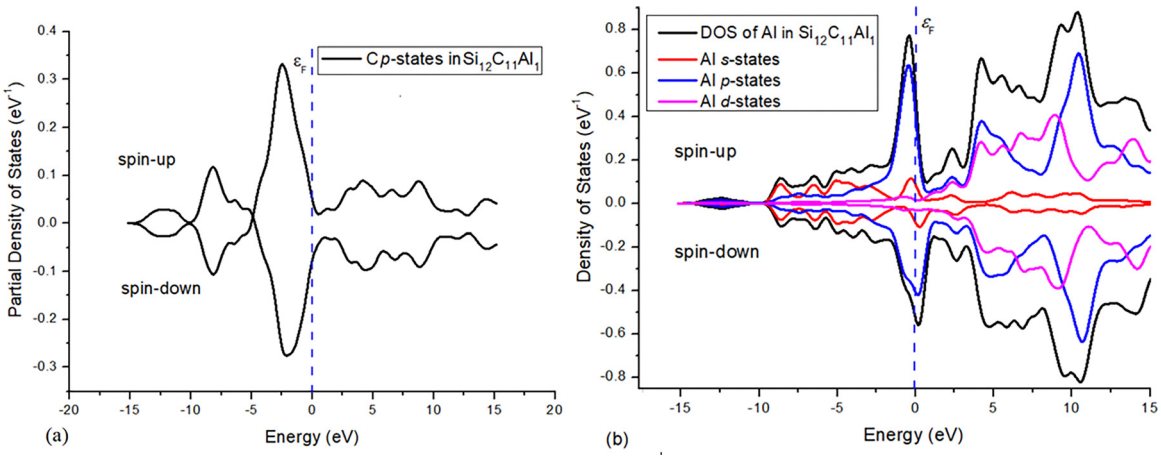

Fig. 8 (a) PDOS of C p-states in $Si_{12}C_{11}Al_1$ NT. (b) PDOS of Al atom showing s, p, and d contributions. Spin-up and spin-down states are shown as positive and negative values, respectively.

The partial density of states (PDOS) for C ans Al atoms in $Si_{12}C_{11}Al_1$, presented in Fig. 8, reveals the origin of the states near the Fermi level. Specifically, the spin-polarized PDOS shows that the carbon p-orbitals and aluminum d-orbitals contribute significantly to the electronic states close to the Fermi level. This orbital hybridization induces magnetism and affects the electronic transport characteristics of the nanotube.

This site-specific doping modifies the spin-polarized electronic behavior of the system, leading to an asymmetric band structure that hints at potential spin-filtering effects. Unlike substitution at the Si site, Al doping at the C site does not induce metallicity but preserves semiconducting behavior in both spin channels. Therefore, such doping configurations may be suitable for applications in nanoscale devices where controlled band gap and spin-resolved conductance are desirable.

Table 3 summarizes the calculated spin-resolved band gap values and electronic properties of the SWSiCNT doped with Al at the C site.

Aluminum substitution at the carbon site in SWSiCNT significantly modifies the electronic and magnetic properties of the system. While the undoped nanotube is a conventional semiconductor with a symmetric band structure, doping introduces spin polarization and band gap asymmetry. As the concentration of dopants increases, the spin-down band gap narrows, approaching half-metallic behavior, this is a promising feature for spintronic and magnetic sensing applications.

To investigate the local electronic effects of aluminum substitution at the carbon site in the SiC nanotube, Bader charge analysis was performed. The results provide insight into charge redistribution and bonding characteristics due to the presence of the Al dopant.

In the $SiC_{1-x}Al_x$ system, where Al replaces a carbon atom, the dopant atom (Al, atom #14) exhibits a net Bader charge of approximately $-1.26e$, indicating electron donation to the surrounding lattice. This charge is significantly lower than that of typical carbon atoms in pristine SiC nanotubes, which generally carry positive Bader charges around $+2.30e$ due to their electron-accepting behavior. The silicon atoms (atoms #11 and #13) located adjacent to the Al dopant site carry charges of about $-1.17e$ and $-1.14e$, respectively. These values are less negative than those of the remaining silicon atoms in the structure, which mostly exhibit charges in the range of $-2.31e$ to $-2.36e$. This local deviation suggests that the Al substitution at the C site disrupts the usual charge distribution and weakens the typical covalent bonding pattern.

The reduced electron transfer from Al to the surrounding Si atoms, compared to what is observed when C is present at that site, reflects the relatively weaker bonding interaction between Al and Si. This modification in local bonding likely influences both the electronic and magnetic properties of the system, particularly in terms of density of states near the Fermi level. The full atomic charge distribution and Bader volumes for the Al-doped (C site) system are included in SI2.

In summary, Bader charge analysis for the $SiC_{1-x}Al_x$ nanotube system reveals that when aluminum replaces a carbon atom, it acts as an electron donor, exhibiting a significantly lower positive charge compared to typical C atoms in the pristine structure. The neighboring Si atoms also show reduced charge transfer, indicating a weakening of local bonding. This redistribution of charge highlights the impact of Al doping at the C site on the electronic structure and supports the observed changes in electronic and magnetic behavior. These findings further underscore the potential of site-specific doping strategies to tailor the properties of SiC nanotubes for advanced spintronic applications.

3.4. Electronic properties of $SiC_{1-x}Ga_x$ NT

The influence of Ga doping at the carbon site in the (6,0) single-walled silicon carbide nanotube (SWSiCNT) was examined to explore spin-dependent electronic behavior. The calculated band structures and total density of states (TDOS) for spin-up and spin-down configurations are shown in Fig. 9. In the case of single Ga substitution at the C site, with a doping concentration of 8.3%, the spin-up and spin-down band gaps were found to be approximately 0.44 eV and 0.60 eV, respectively.

Table 3 Calculated spin-up (↑) and spin-down (↓) band gaps of Al-doped SWSiCNTs at different doping concentrations (C site substitution)

System	Doping level (%)	Band gap (eV)	Electronic nature	Remarks
SWSiCNT (undoped)	0	0.98	Semiconductor	Pristine nanotube; reference system[21]
SWSiCNT (Al at C site)	8.3	0.66 (↑), 0.51 (↓)	Spin-asymmetric semiconductor	Doping introduces magnetic moment and band gap asymmetry
SWSiCNT (2 Al at C sites)	16.6	0.60 (↑), 0.12 (↓)	Strongly spin-polarized semiconductor	Spin-down channel nearly metallic; potential for spintronic applications

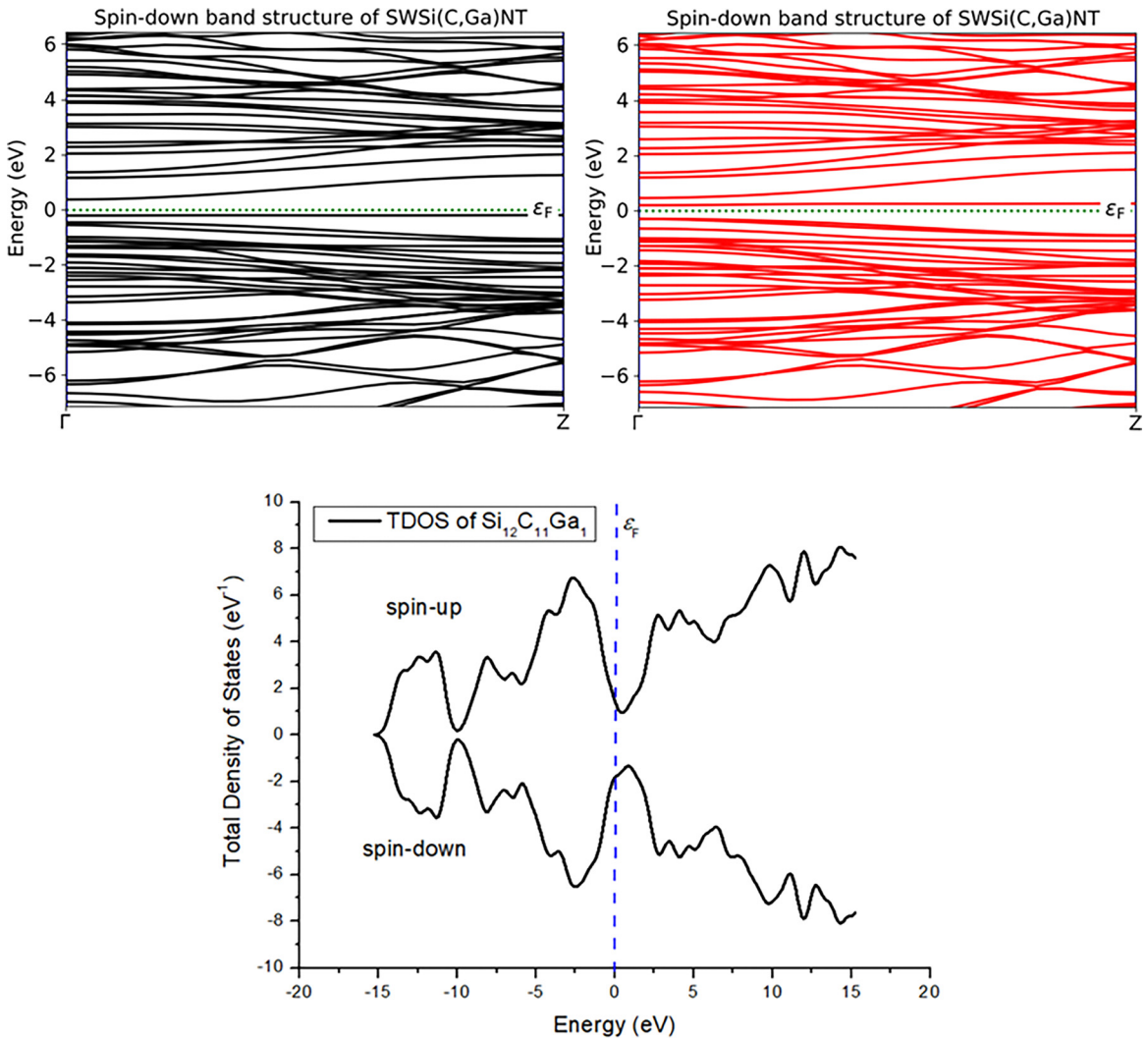

Fig. 9 The calculated spin-up (black) and spin-down (red) band structures, and TDOS diagram for $SiC_{1-x}Ga_x$ NTs.

This asymmetry in the electronic band gaps indicates spin-polarized semiconducting behavior, suggesting potential applications in spintronic devices. When the doping concentration was increased to 16.6% by introducing a second Ga atom at another carbon site, the band gap was further reduced to 0.26 eV for both spin channels, indicating enhanced interaction between dopant atoms and a shift toward narrower semiconducting behavior.

The partial density of states (PDOS) from the C and Ga atoms is illustrated in Fig. 10, showing the contributions of the Ga s-, p-, and d-orbitals and the C p-states to the overall electronic structure. The positive and negative DOS values represent majority and minority spin states, respectively, further confirming the spin-resolved characteristics of the doped systems. The band structures and TDOS of the double Ga-doped configuration (16.6%) are provided in SI1.

Table 4 presents a summary of the calculated spin-up and spin-down band gaps for Ga-doped SWSiCNTs at different doping concentrations, along with their corresponding electronic character and remarks.

Table 4 shows that increasing Ga doping from 8.3% to 16.6% at the carbon site in SWSiCNTs changes the electronic

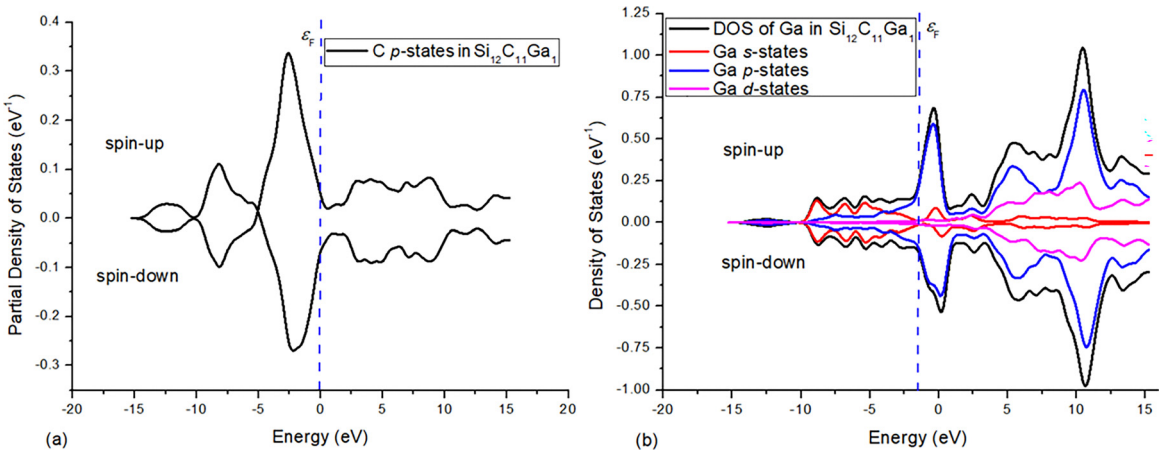

Fig. 10 Calculated PDOS for the C (a) and Ga (b) atoms for $SiC_{1-x}Ga_x$ NTs. Positive and negative DOS values represent majority and minority spin states, respectively.

Table 4 Calculated spin-up (↑) and spin-down (↓) band gaps of Ga-doped SWSiCNTs at different doping concentrations

System	Doping level (%)	Band gap (eV)	Electronic nature	Remarks
SWSiCNT (undoped)	0	0.98	Semiconductor	Previous work[21]
SWSiCNT (Ga at C site)	8.3	0.44 (↑), 0.60 (↓)	Spin-polarized semiconductor	Spin asymmetry observed; both channels retain band gaps
SWSiCNT (2 Ga at C sites)	16.6	0.26 (↑), 0.26 (↓)	Narrow-gap semiconductor	Spin symmetry restored; reduced gap suggests dopant-induced band edge shift

properties noticeably. At 8.3%, the system is spin-asymmetric with band gaps of 0.44 eV (spin-up) and 0.60 eV (spin-down), indicating spin polarization. At 16.6%, the band gaps equalize at 0.26 eV, reflecting restored spin symmetry and reduced gap, likely due to stronger dopant-dopant interactions and orbital hybridization. The partial DOS analysis further supports this conclusion by showing significant contributions from both Ga and C orbitals near the Fermi level. These findings confirm that higher Ga doping at C site in the SWSiCNT not only narrows the band gap but also modifies the spin characteristics of the system, demonstrating the tunability of the electronic structure through controlled doping, a key requirement for spintronic and nanoelectronic applications.

The Bader charge analysis of the $SiC_{1-x}Ga_x$ nanotube system, where gallium substitutes a carbon atom, reveals significant changes in charge distribution. The Ga atom exhibits a substantially lower positive charge ($-0.71|e|$) compared to that of carbon atoms in the pristine structure ($\sim+2.3|e|$), indicating its role as a weak electron donor. The neighboring Si atoms also display reduced charge transfer, suggesting weakened local bonding interactions. This redistribution of charge aligns with the observed alterations in the electronic structure, supporting the emergence of spin polarization and modified electronic behavior. These results highlight the effectiveness of Ga doping at the C site in tuning the electronic properties of SiC nanotubes for potential spintronic applications. A full table of Bader charges for the Ga-doped SWSiCNT at C site is provided in SI2.

3.5. Magnetic properties of $Al_xSi_{1-x}C$ NT

In this section, we studied the magnetic properties of the Al-doped SiCNT system, specifically when Al substitutes a Si site. To explore the magnetic behavior, we calculated the magnetic moments of all atoms and estimated the total magnetic moment of the system. Additionally, we investigated the relative stability of the ferromagnetic (FM) and antiferromagnetic (AFM) phases to determine the energetically favorable magnetic configuration. To gain further insight into the origin of magnetism and the nature of charge redistribution, we visualized the electron difference density. These isosurface plots clearly show how the electronic charge distribution is altered due to doping, particularly highlighting the local interactions between the Al dopant and the surrounding Si and C atoms. The combination of spin-polarized electronic structure, magnetic moment analysis, and charge density visualization provides a comprehensive understanding of the magnetic response induced by Al doping in the SiCNT system.

The Mulliken population analysis for the sinle Al-doped (6,0) SiC nanotube at Si site reveals a total spin magnetic moment of approximately $1.0\mu_B$, indicating the presence of net spin polarization induced by the Al substitution at a silicon site. Fig. 11 shows the spin-polarization distribution for the one Al-doped at Si site in SiC nanotube, where the green arrows indicate the magnitude and direction of the local magnetic moments. Spin polarization view for double Al-doped at Si sites in SWSiCNT is shown in SI3.

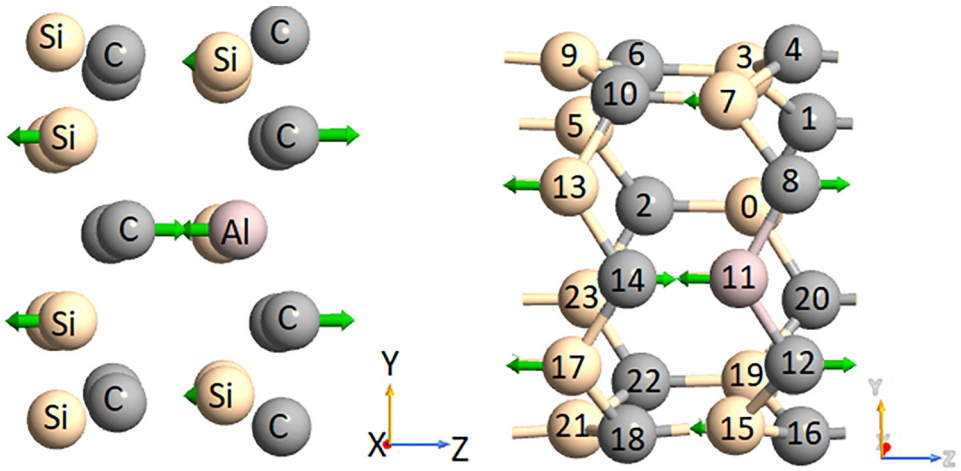

Fig. 11 Spin polarization views in $Al_xSi_{1-x}C$ NT. The spin-polarization distribution in the Al-doped SiC nanotube is illustrated, where the green arrows indicate the direction and magnitude of the local magnetic moments.

Table 5 shows the spin magnetic moments for a single Al atom doped at a silicon site in the (6,0) SiC nanotube. In this case, the total magnetic moment is approximately $1.0\mu_B$.

The Al dopant carries a strong negative spin moment of about $-2.64\mu_B$, indicating an antiferromagnetic coupling with neighboring atoms. Several nearby carbon atoms, such as C8 ($2.03\mu_B$), C12 ($1.92\mu_B$), and C14 ($2.72\mu_B$), exhibit large positive spin moments, partially compensating the Al's negative moment. Silicon atoms mostly show small negative spin moments. The Al dopant carries a strong negative spin magnetic moment of approximately $-2.64\mu_B$, indicating an antiferromagnetic interaction with its neighboring atoms. This negative contribution is partially balanced by several silicon atoms nearby that exhibit significant negative spin moments, such as Si7 ($-0.60\mu_B$), Si13 ($-1.14\mu_B$), Si15 ($-0.60\mu_B$), and Si17 ($-1.17\mu_B$). The remaining silicon atoms show smaller spin moments, mostly negative and close to zero, indicating weaker spin polarization farther from the dopant.

Table 5 Spin magnetic moments (in Bohr magnetons) of atoms in single and double Al-doped (6,0) SiC NTs at silicon sites

No.	Element	Spin moment (1 Al-doped)	Spin Moment (2 Al-doped)
0	Si/Al	0.028 (Si)	−0.068 (Al)
1	C	−0.058	0.250
2	C	0.002	0.143
3	Si	−0.087	0.037
4	C	0.308	0.039
5	Si	−0.012	0.007
6	C	0.067	−0.304
7	Si	−0.596	−0.022
8	C	2.027	−0.022
9	Si	−0.111	0.012
10	C	0.088	0.020
11	Al	−2.644	0.055 (Al)
12	C	1.915	0.099
13	Si	−1.136	−0.009
14	C	2.724	0.280
15	Si	−0.603	−0.028
16	C	0.136	0.144
17	Si	−1.170	−0.038
18	C	0.289	−0.045
19	Si	−0.033	−0.021
20	C	−0.049	−0.075
21	Si	−0.113	−0.055
22	C	0.035	0.135
23	Si	−0.003	−0.014
	Sum	1.002	0.520

In contrast, when two Al atoms are doped simultaneously at silicon sites (double Al doping), the total spin magnetic moment decreases to around $0.52\mu_B$. Here, the Al atoms themselves have very small spin moments ($-0.07\mu_B$ and $0.06\mu_B$), indicating a weaker direct magnetic contribution. The surrounding carbon and silicon atoms display relatively small positive and negative spin moments, reflecting a more balanced spin distribution and weaker overall magnetization. This comparison indicates that single Al doping at a silicon site induces stronger local spin polarization and a higher net magnetic moment compared to double Al doping at silicon sites, where magnetic moments are more compensated, resulting in a lower total magnetization.

A detailed orbital-specific Mulliken population analysis provides insight into which atomic orbitals contribute most to the observed magnetism. Silicon atoms generally show significant spin populations in their 3p orbitals (labeled y, z, x), with values around 0.6 to 0.7 electrons, reflecting a strong involvement of p orbitals in both bonding and spin polarization. Their 3s orbitals also contribute with smaller but notable spin densities around 1.0 electron, while minor contributions arise from d-like orbitals (*e.g.*, xy, zy, zz–rr), with population values ranging from approximately 0.01 to 0.1. Carbon atoms display pronounced spin polarization primarily in their 2p orbitals (y, z, x), typically between 0.5 and 0.9 electrons, with smaller contributions from the 2s orbitals ($\sim$0.6 electrons). Additionally, minor but non-negligible populations appear in d-like orbitals, indicating slight hybridization with orbitals of higher angular momentum.

The Al dopant itself shows spin populations in the 3p orbitals ranging from about 0.1 to over 1.1 electrons,

Table 6 Spin magnetic moments (in Bohr magnetons) of atoms in single and double Ga-doped (6,0) SiC NTs at silicon sites

No.	Element	Spin moment (1 Ga-doped)	Spin moment (2 Ga-doped)
0	Si	−0.002	−0.574 (Ga)
1	C	−0.001	1.036
2	C	0.010	0.474
3	Si	−0.028	−0.582
4	C	0.095	0.891
5	Si	−0.006	−0.376
6	C	0.011	0.153
7	Si	−0.167	−0.582
8	C	0.183	1.036
9	Si	−0.137	−0.253
10	C	0.408	0.154
11	Ga	−0.336	−0.573
12	C	0.183	1.035
13	Si	−0.500	−0.375
14	C	1.612	0.470
15	Si	−0.167	−0.582
16	C	0.095	0.892
17	Si	−0.500	−0.375
18	C	0.408	0.154
19	Si	−0.028	−0.582
20	C	−0.001	1.036
21	Si	−0.137	−0.253
22	C	0.011	0.154
23	Si	−0.006	−0.376
	Sum	1.001	2.002

Table 8 Spin magnetic moments (in Bohr magnetons) of individual atoms in single and double Ga-doped (6,0) SiC NTs at carbon sites

No.	Element	Spin moment, μ_B (1 Ga-doped)	Spin moment, μ_B (2 Ga-doped)
0	Si	−0.022	−0.715
1	C	0.017	1.986
2	C/Ga	0.031 (C)	0.041 (Ga)
3	Si	−0.042	−1.248
4	C	0.101	2.656
5	Si	−0.029	−0.603
6	C	0.043	0.845
7	Si	−0.144	−1.189
8	C	0.250	1.914
9	Si	−0.090	−0.892
10	C	0.219	0.811
11	Si	0.044	−0.801
12	C	0.250	1.914
13	Si	−0.121	−0.559
14	Ga	0.541	0.039 (Ga)
15	Si	−0.144	−1.189
16	C	0.101	2.656
17	Si	−0.121	−0.559
18	C	0.219	0.811
19	Si	−0.042	−1.248
20	C	0.017	1.986
21	Si	−0.090	−0.892
22	C	0.043	0.845
23	Si	−0.029	−0.603
	Sum	1.0	6.0

highlighting the important role of these orbitals in the magnetic behavior of Al. Smaller spin populations are present in the 3s orbital ($\sim$0.05 electrons), as well as in d-like orbitals such as *xy*, *zy*, and *zz–rr*. The dominant spin polarization on the carbon 2p orbitals near the Al site indicates that these orbitals are primarily responsible for the induced magnetic moment in the system. The Al 3p orbitals contribute significantly to the negative spin moment on the dopant, suggesting weaker hybridization and spin-dependent charge transfer with neighboring atoms. Silicon atoms display a mixed behavior, with negative spin moments mainly localized in the p orbitals, which supports antiferromagnetic coupling between Si and Al atoms.

Table 7 Spin magnetic moments (in Bohr magnetons) of atoms in single and double Al-doped (6,0) SiC NTs at carbon sites

No.	Element	Spin moment (1Al-doped)	Spin moment (2Al-doped)
0	Si	−0.003	−0.787
1	C	−0.001	1.978
2	C/Al	0.011 (C)	0.452 (Al)
3	Si	−0.024	−1.317
4	C	0.085	2.992
5	Si	−0.009	−0.676
6	C	0.019	1.357
7	Si	−0.119	−1.315
8	C	0.225	1.989
9	Si	−0.066	−1.105
10	C	0.173	1.349
11	Si	0.025	−0.782
12	C	0.225	1.989
13	Si	−0.102	−0.672
14	Al	0.604	0.446
15	Si	−0.119	−1.315
16	C	0.085	2.992
17	Si	−0.102	−0.672
18	C	0.173	1.349
19	Si	−0.024	−1.317
20	C	−0.001	1.978
21	Si	−0.066	−1.105
22	C	0.019	1.357
23	Si	−0.009	−0.676
	Sum	1.001	8.488

The presence of spin populations in d-like orbitals (*xy*, *zy*, *zz–rr*, *zx*, *xx–yy*) on all atoms implies some degree of orbital hybridization beyond simple s and p orbitals, contributing to the overall magnetic character. For example, the s orbital typically shows a slight spin polarization (*e.g.*, around $-0.013\mu_B$), while the p orbitals contribute small negative moments, indicating a slightly higher number of spin-down electrons. The total atomic spin magnetic moment is thus the sum of all orbital contributions.

Overall, the magnetic moment in the system is mainly localized on specific carbon atoms surrounding the Al dopant, while the Al atom and neighboring silicon atoms show negative spin polarization. This distribution suggests antiferromagnetic coupling between the Al dopant and the Si atoms, with the induced magnetism largely centered on the carbon atoms, resulting in a net magnetic moment close to $1\mu_B$.

Fig. 12 shows the spin-polarized DOS for the three carbon atoms chemically bonded to the Al dopant. The asymmetry between the spin-up and spin-down states clearly reflects strong spin polarization, confirming the dominant role of these carbon atoms in the induced magnetic behavior of the Al-doped SiC nanotube.

Fig. 13 illustrates the spin density isosurface plot, representing how the electronic charge distribution changes when an Al atom substitutes a Si atom in the SWSiCNT structure. The

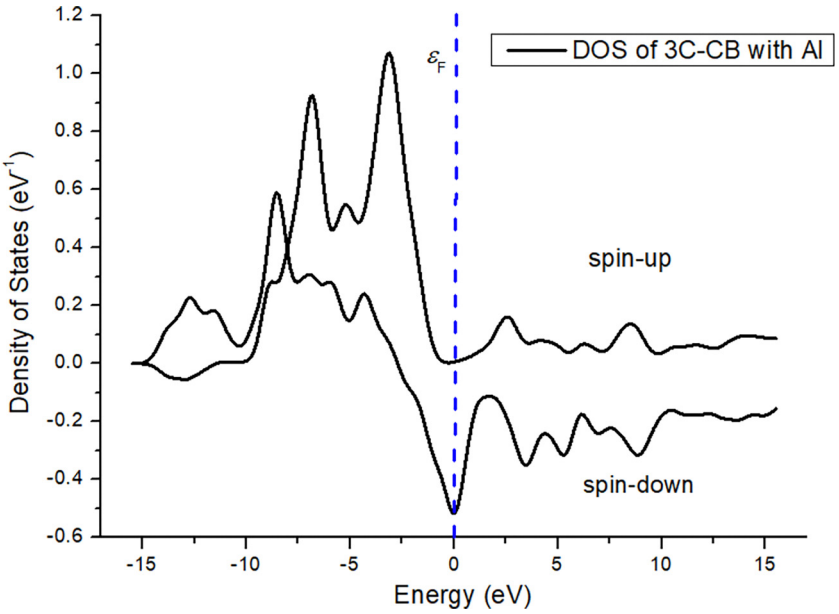

Fig. 12 Spin-polarization DOS diagrams for 3C atoms chemically bonded (CB) with dopant in $Al_xSi_{1-x}C$ NT.

beige, gray, and pink spheres represent silicon (Si), carbon (C), and aluminum (Al) atoms, respectively. The positive values (purple) indicate areas where electrons accumulate, mainly around the dopant and neighboring carbon atoms, while negative values (cyan) show regions of electron depletion, primarily around the replaced Si sites. This redistribution reveals the nature of bonding and charge transfer between Al and the host nanotube lattice, providing insight into the electronic effects caused by doping at the atomic level. The strong interaction and partial charge transfer highlighted in this visualization help explain the changes observed in the electronic and magnetic properties of the doped SiC nanotube.

To investigate the magnetic ground state of the $Al_xSi_{1-x}C$ nanotube, we calculated the total energies of both FM and AFM configurations. The total energy of the FM state was found to be −3891.47261 eV, while that of the AFM state was −3912.51781 eV. The positive energy difference between these two states indicates that the AFM configuration is energetically more favorable. Therefore, for the Al-doped (6,0) SWSiCNT system, the antiferromagnetic phase is more stable than the ferromagnetic one.

3.6. Magnetic properties of $Ga_xSi_{1-x}C$ NT

In this section, we examined the magnetic properties of the Ga-doped SiCNT system, focusing on the case where a Ga atom replaces a Si site. To analyze the magnetic behavior introduced by Ga doping, we computed the magnetic moments of all atoms and evaluated the total magnetic moment of the system. Furthermore, we compared the ferromagnetic (FM) and antiferromagnetic (AFM) configurations to identify the most energetically stable magnetic phase. To better understand the origin of the magnetism and the local electronic environment, we visualized the electron difference density. The resulting

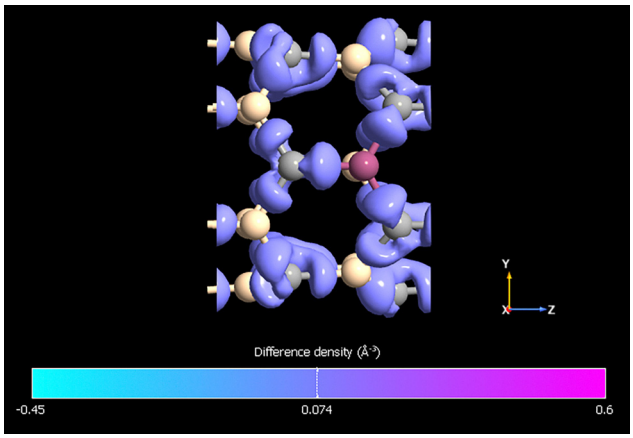

Fig. 13 Spin density isosurface plot for Al doped at the Si site in SWSiCNT. The plot highlights the charge redistribution upon doping, where regions of charge accumulation are shown in purple and charge depletion in cyan, indicating the local electronic interaction between the Al dopant and surrounding atoms.

isosurface plots illustrate the charge redistribution caused by Ga doping, especially emphasizing the interaction between the Ga dopant and nearby Si and C atoms. This integrated analysis of spin-polarized electronic structure, magnetic moment distribution, and local charge transfer offers a detailed understanding of how Ga doping affects the magnetic characteristics of the SiCNT system.

The Mulliken spin magnetic moment results indicate that the Ga-doped (6,0) SiC nanotube exhibits a total magnetic moment of approximately $1.0\mu_B$, confirming the emergence of spin polarization upon single Ga substitution at Si site (Fig. 14). Spin polarization view for double Ga-doped at Si sites in SWSiCNT is shown in SI3.

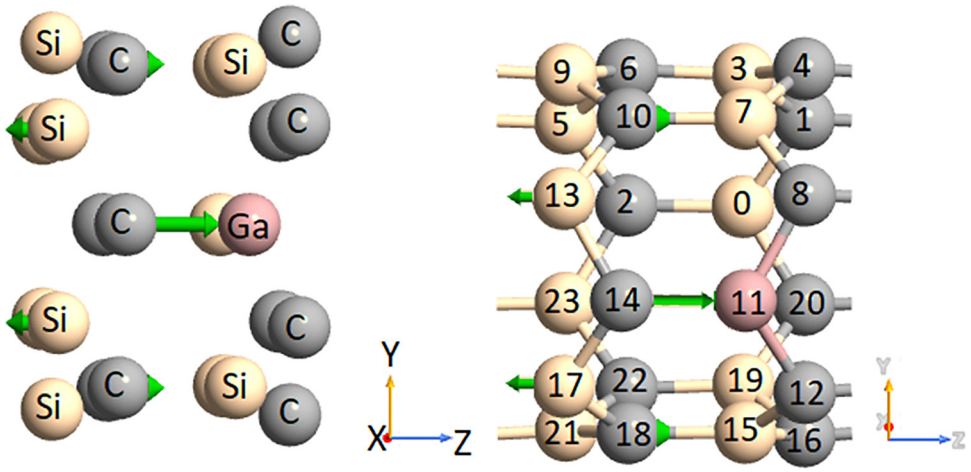

Fig. 14 Spin-polarization views of $SiC_{1-x}Ga_x$ NT. The green arrows represent the magnetic moments.

In the case of a single Ga-doped SiCNT, the overall magnetic moment sums to approximately $1.0\mu_B$, indicating a net ferromagnetic moment induced by the presence of one Ga dopant. The Ga atom itself carries a negative spin magnetic moment of $-0.336\mu_B$, acting as a localized magnetic impurity that influences the spin environment of its neighboring atoms. The largest positive contributions to the total magnetization come from nearby carbon atoms, particularly C14, which exhibits a significant magnetic moment of about $1.6\mu_B$, suggesting strong local spin polarization. Additionally, carbon atoms C10 and C18 each contribute over $0.4\mu_B$, underscoring the important role of carbon atoms in hosting induced magnetic moments. Neighboring silicon atoms also show substantial negative spin moments, with Si13 and Si17 each having around $-0.5\mu_B$, indicating antiferromagnetic-like coupling with the positively polarized carbon atoms. These results imply that the induced magnetism is primarily localized on specific carbon atoms surrounding the Ga dopant, while the negative moments on Si and Ga sites partially compensate the overall magnetization. This distribution reflects a complex interplay of spin polarization and hybridization effects, whereby Ga doping enhances magnetic polarization on carbon atoms and simultaneously induces antiparallel spin alignment in adjacent silicon atoms.

When two Ga atoms are introduced into the SiCNT, the total spin magnetic moment increases to approximately $2.002\mu_B$, nearly doubling the magnetic moment observed in the single-doped case. This suggests largely additive magnetic contributions from each dopant. Both Ga atoms exhibit larger negative spin moments of about $-0.57\mu_B$, indicating stronger magnetic impurity effects than in the single-doped system. Several carbon atoms adjacent to the Ga dopants, including sites 1, 4, 8, 12, and 20, show enhanced positive spin moments close to or exceeding $1.0\mu_B$, pointing to increased spin polarization in the carbon sublattice. Silicon atoms maintain negative magnetic moments, though some show reduced magnitudes compared to the 1 Ga-doped scenario, possibly due to overlapping spin polarization fields created by multiple dopants, leading to more complex magnetic interactions. The spatial extension of induced spin moments around each Ga dopant likely overlaps, resulting in stronger net magnetization but also subtle compensatory effects that modulate local moments. These findings highlight that magnetism in Ga-doped SiCNTs arises from a delicate balance between localized magnetic moments on Ga impurities and induced spin polarization in the surrounding carbon network, with silicon atoms playing an essential role in mediating these interactions.

The orbital analysis highlights a notable redistribution of electronic charge and spin polarization, particularly around the Ga dopant and its neighboring atoms. Among the three carbon atoms bonded to Ga, there is a significant occupation of p orbitals, especially the p_x and p_y components which aligns with their substantial positive spin magnetic moments observed earlier. Ga itself shows dominant occupation in s and p orbitals, but with comparatively smaller spin contributions, reflecting its role as an electron acceptor and weakly magnetic center. Surrounding silicon atoms generally exhibit negative spin polarization, mainly from their p orbitals, which compensates for the spin accumulation on adjacent carbon atoms and contributes to the overall magnetic behavior of the system.

Table 6 presents the calculated spin magnetic moments (in Bohr magneton, μ_B) of individual atoms in SiCNTs doped with one and two gallium (Ga) atoms substituting silicon (Si) sites. The doping-induced changes in the magnetic moments reveal how the presence of Ga affects the magnetic properties of the SiCNT system.

Overall, the data clearly demonstrate that carbon atoms are critical in sustaining and amplifying the magnetization induced by Ga doping, with specific carbon sites exhibiting notably high spin magnetic moments. The negative spin moments observed on Ga and Si atoms indicate antiferromagnetic coupling that partially offsets the positive moments on carbon, resulting in a net magnetic moment that is less than the simple sum of absolute values. The approximately linear increase in total magnetization when moving from one to two Ga dopants suggests that magnetic contributions from individual Ga atoms and their surrounding carbon environment

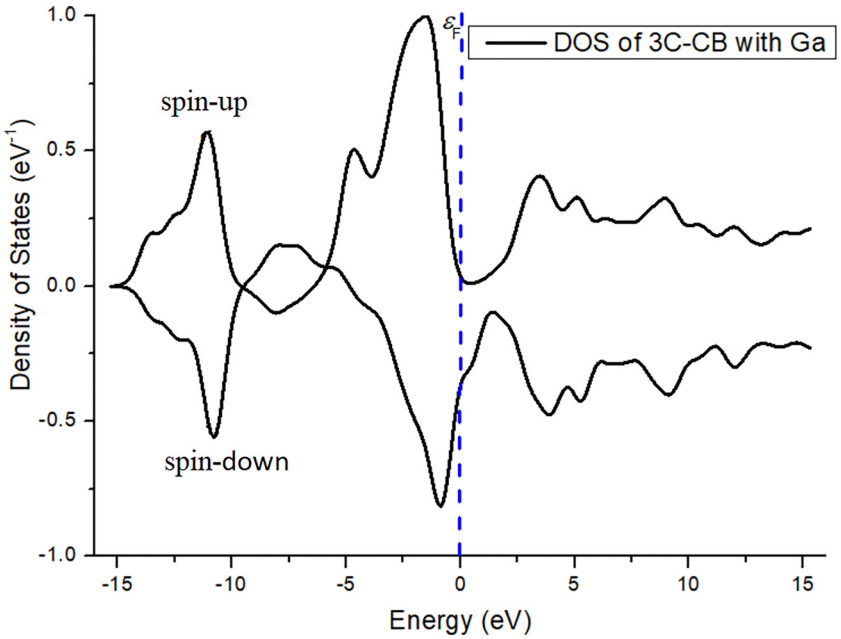

Fig. 15 Spin-polarization DOS diagrams for 3C atoms chemically bonded (CB) with dopant in $Ga_xSi_{1-x}C$ NT.

largely add constructively without significant magnetic quenching. This behavior is promising for potential spintronic applications, where controlled doping could be used to tune the magnetic properties of SiCNTs to achieve desired spin configurations. Furthermore, the results emphasize the importance of local atomic environments and dopant concentration in tailoring magnetism within low-dimensional semiconductor nanostructures.

Fig. 15 presents the spin-polarized DOS diagrams for the three carbon atoms chemically bonded to the Ga dopant. The noticeable asymmetry between the spin-up and spin-down states indicates strong spin polarization, highlighting the key role of these carbon atoms in the magnetic behavior induced by Ga doping in the SiC nanotube.

Fig. 16 illustrates how the electronic charge density is redistributed when a gallium (Ga) atom substitutes a silicon (Si) atom in the SWSiCNT. The purple regions denote electron accumulation, mainly concentrated around the Ga dopant and adjacent carbon atoms, reflecting areas of increased electron density. Conversely, the cyan regions indicate electron depletion, mostly observed near the replaced Si site. This pattern of charge transfer and redistribution reveals the nature of bonding between the Ga dopant and the host nanotube lattice, providing important insight into how doping alters the local electronic environment and influences the overall electronic properties of the system.

The total energy difference between the FM and AFM states is found to be positive, with energies of −4108.82776 eV for the FM state and −4108.92690 eV for the AFM state. This indicates that the AFM configuration is energetically more favorable, suggesting that the Ga-doped (6,0) SWSiCNT prefers an antiferromagnetic ground state. The presence of such magnetic ordering in Ga-doped SWSiCNTs highlights their potential as nanoscale magnetic materials, making them promising candidates for spintronic and nanomagnetic device applications.

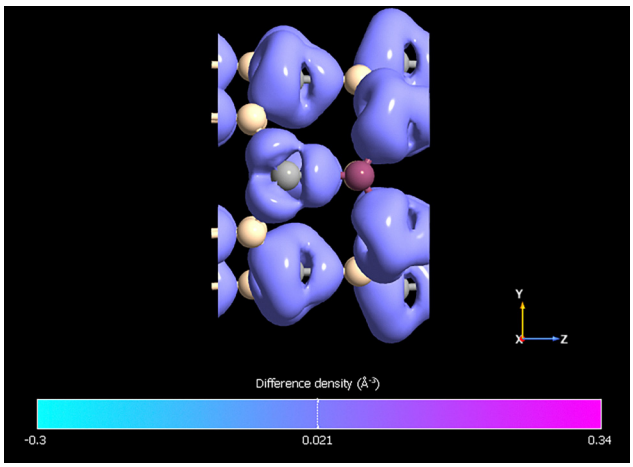

Fig. 16 Spin density isosurface plot for Ga doped at the Si site in SWSiCNT. The plot highlights the charge redistribution upon doping, where regions of charge accumulation are shown in purple and charge depletion in cyan, indicating the local electronic interaction between the Ga dopant and surrounding atoms. Beige, gray, and pink spheres represent silicon (Si), carbon (C), and gallium (Ga) atoms, respectively.

3.7. Magnetic properties of $SiC_{1-x}Al_xNT$

In this section, we investigate the magnetic properties of the SiCNT system when Al atoms are doped at carbon sites. Spin-polarized DFT calculations were performed to determine the magnetic moments on each atom and the total magnetic moment of the system. Additionally, the relative stability between the ferromagnetic (FM) and antiferromagnetic (AFM) configurations was evaluated. To gain insight into the magnetic

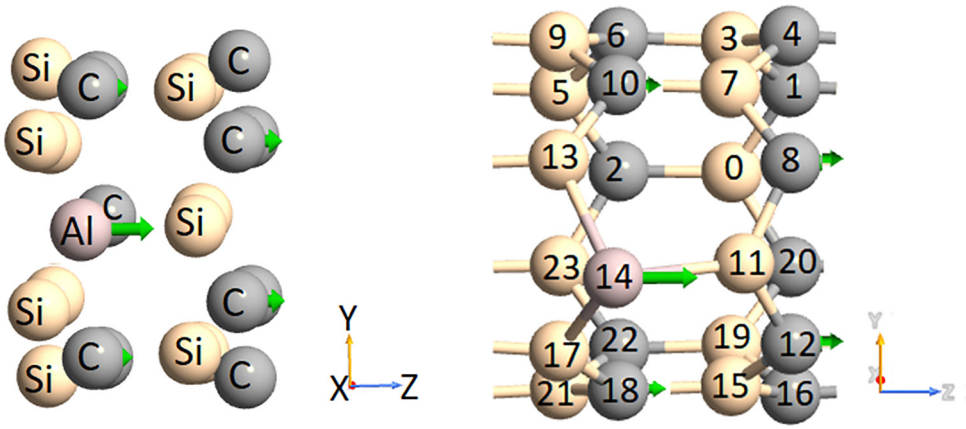

Fig. 17 Spin polarization in $SiC_{1-x}Al_x$ NT. The spin-polarization distribution in the Al-doped SiC nanotube is illustrated, where the green arrows indicate the direction and magnitude of the local magnetic moments.

origin and electronic redistribution, electron difference density plots were generated. These visualizations highlight how Al substitution at C sites affects local charge accumulation and depletion, revealing the nature of bonding and magnetic interaction in the doped system.

The introduction of Al dopants into the SiC nanotube lattice significantly alters its magnetic behavior. The spin-polarized charge density and DOS analyses reveal localized magnetic moments and spin asymmetry, indicative of induced magnetism due to the presence of the Al impurity. Fig. 17 illustrates the spin-polarization distribution in the single Al-doped $SiC_{1-x}Al_x$ NT. Spin polarization view for double Al-doped at carbon sites in SWSiCNT is shown in SI3.The green arrows represent the direction and magnitude of local magnetic moments. It is evident that the magnetization is localized primarily on the carbon atoms neighboring the aluminum dopant and the nearby silicon atoms. This magnetic moment arises due to the unpaired electrons resulting from the substitution of a trivalent Al atom in place of a tetravalent Si atom, introducing holes into the system and breaking the spin symmetry.

Table 7 shows the spin magnetic moments (in Bohr magnetons) of individual atoms in single and double Al-doped (6,0) SiC nanotubes with Al substituting by carbon atom. The single Al-doped case exhibits a total magnetic moment of approximately $1.0\mu_B$, indicating moderate spin polarization localized near the Al dopant and adjacent atoms. In contrast, the double Al-doped case shows a significantly higher total magnetic moment of about $8.488\mu_B$, reflecting a stronger spin polarization and enhanced magnetic interactions due to the presence of two Al atoms. In both doping configurations, the Al atoms carry positive spin moments ($\sim$0.45–0.60μ_B), directly

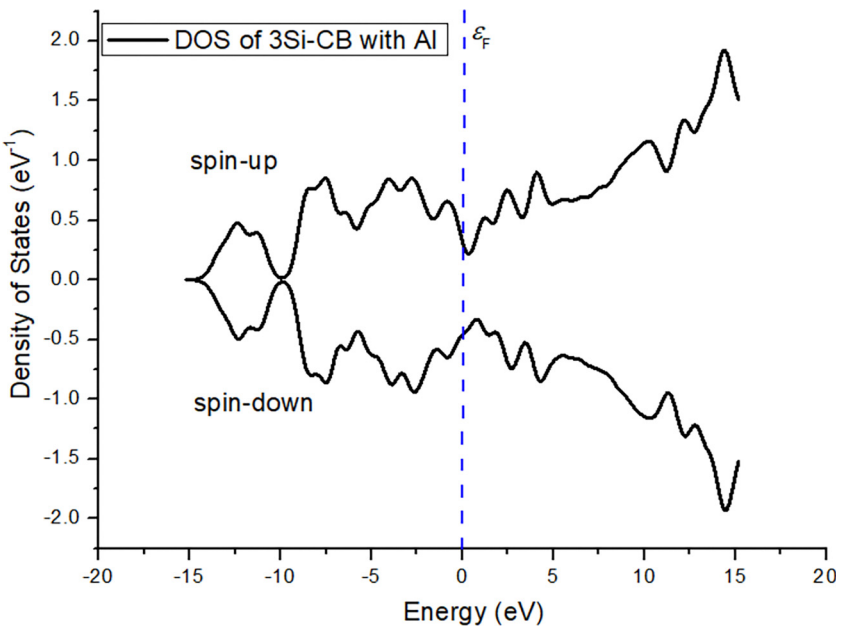

Fig. 18 Spin-polarization DOS diagrams for 3Si atoms chemically bonded (CB) with dopant in $SiC_{1-x}Al_x$ NT.

contributing to the overall magnetization. The neighboring carbon atoms display large positive spin moments, especially in the double-doped case where atoms such as C4, C8, C12, and C16 have moments approaching $3.0\mu_B$, indicating strong localization of magnetic moments on carbon sites. Silicon atoms exhibit mostly negative spin moments, consistent with antiferromagnetic coupling to the Al dopants. The comparison reveals that increasing the number of Al dopants significantly amplifies the total spin magnetic moment and the degree of spin polarization within the nanotube structure.

The spatial distribution of spin density indicates a ferromagnetic alignment in the vicinity of the Al dopant. The local magnetic moments are predominantly aligned in one direction (spin-up), showing a net magnetic moment, which confirms that the Al dopant induces a significant magnetic response in the SiC nanotube structure.

Fig. 18 presents the spin-polarized DOS for the system containing three Si atoms chemically bonded with the Al dopant in $SiC_{1-x}Al_x$ NT. The spin-up and spin-down DOS curves show a clear asymmetry near the Fermi level, indicated by the vertical dashed line at 0 eV, confirming the presence of spin polarization in the system.

Notably, there is a finite density of states at the Fermi level for the spin-up channel, while the spin-down channels shows a reduced or nearly zero DOS at the Fermi level. This spin asymmetry implies that the system may exhibit half-metallic behavior, which is a desirable property for spintronic applications. In such systems, electrons of only one spin orientation contribute to conduction, allowing for 100% spin-polarized current. The magnetism in this Al-doped SiC nanotube system arises from the electronic imbalance introduced by the Al dopant, and the interaction with surrounding Si and C atoms. The presence of spin polarization without requiring external magnetic fields or magnetic atoms indicates that Al-doped SiC NTs are promising candidates for intrinsic spintronic materials.

Fig. 19 displays the spin-polarized charge density distribution map for the system where an Al atom substitutes a carbon atom in the SWSiCNT lattice. The plot highlights how charge distribution is altered due to the presence of the Al dopant. The purple (positive) regions show where electrons accumulate, primarily around the aluminum atom and its neighboring silicon atoms, indicating areas of stronger bonding or electron localization. Conversely, the cyan (negative) regions show where electrons have been depleted relative to the undoped structure. This redistribution reflects significant charge transfer from the Al dopant toward adjacent Si atoms, suggesting modified bonding characteristics and altered electronic structure in the vicinity of the dopant site. Such insights are crucial for understanding the effect of doping on the material's electronic and magnetic behavior.

The total energy of the FM and AFM configurations for the Al-doped (6,0) SWSiCNT system, where Al substitutes a carbon site, are calculated to be −3956.66549 eV and −3956.67554 eV, respectively. The energy difference between the two magnetic states is positive, indicating that the AFM configuration is

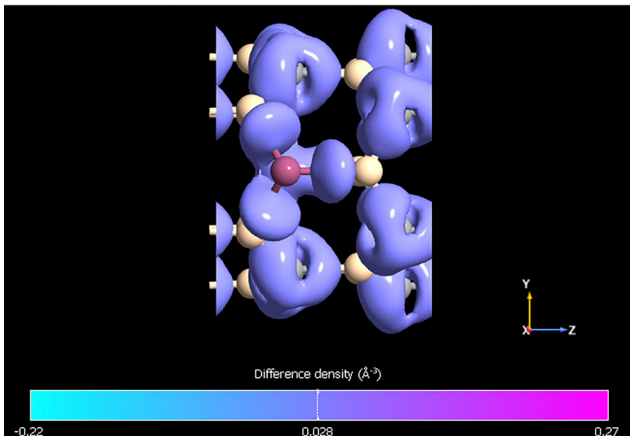

Fig. 19 Spin density isosurface plot for Al doped at the C site in SWSiCNT. The purple regions represent charge accumulation, while cyan regions indicate charge depletion. Beige, gray, and pink spheres denote silicon (Si), carbon (C), and aluminum (Al) atoms, respectively.

energetically more favorable than the FM state. This suggests that the Al(C)-doped SWSiCNT prefers an antiferromagnetic ground state. Such behavior points to the presence of magnetic interactions induced by Al doping, which may be beneficial for the development of nanoscale spintronic devices.

3.8. Magnetic properties of $SiC_{1-x}Ga_x$ NT

In this section, we examine the magnetic properties of the Ga-doped SiCNT system, specifically when Ga replaces a carbon atom. Using spin-polarized DFT calculations, we analyzed the atomic magnetic moments and computed the total magnetic moment of the system. We also compared the energetic stability of ferromagnetic (FM) and antiferromagnetic (AFM) phases to identify the preferred magnetic ground state. To further understand the origin of magnetism and charge redistribution, we visualized the electron difference density. These isosurface plots reveal how Ga doping at the C site modifies the local electronic environment and contributes to the overall magnetic behavior of the nanotube system.

Fig. 20 illustrates the spin polarization distribution in the $SiC_{1-x}Ga_x$ nanotube, where a one Ga atom substitutes for a C atom in the lattice. Spin polarization view for double Ga-doped at carbon sites in SWSiCNT is shown in SI3. Similar to the Al-doped system, the green arrows indicate the direction and magnitude of local magnetic moments. The presence of Ga induces localized magnetic moments in the neighboring carbon atoms, especially those directly bonded to the Ga dopant. This is attributed to the electronic configuration of gallium, which, like aluminum, is trivalent and introduces a hole when replacing a tetravalent Si atom. The charge imbalance from this substitution leads to unpaired electrons in the system, generating spin polarization.

Compared to the Al-doped system, the distribution of magnetic moments in the Ga-doped structure may be somewhat broader or more delocalized, depending on the size and electronegativity differences between Ga and Al. The magnetic

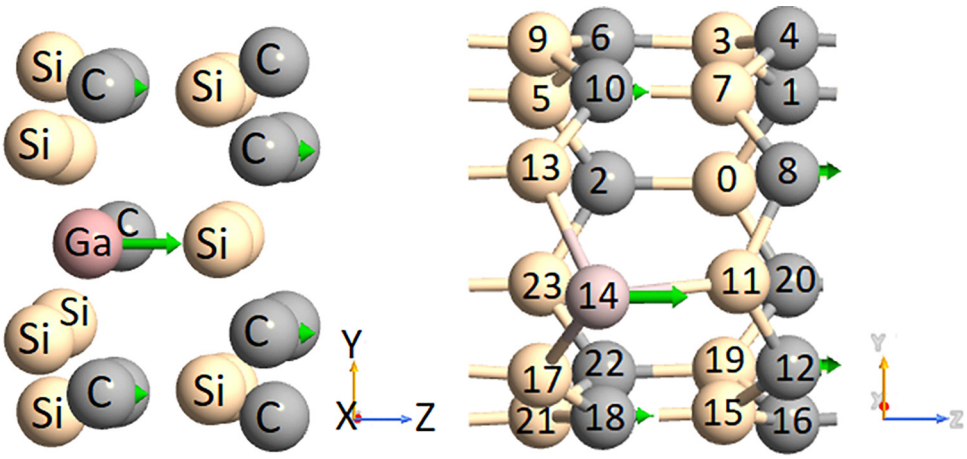

Fig. 20 Spin polarization in $SiC_{1-x}Ga_x$ NT. The spin-polarization distribution in the Ga-doped SiC nanotube is illustrated, where the green arrows indicate the direction and magnitude of the local magnetic moments.

moments are again concentrated around the dopant site, involving both C and nearby Si atoms. The system demonstrates ferromagnetic ordering in the localized region, which suggests that Ga doping, like Al doping, induces intrinsic magnetism in the SiC nanotube without requiring magnetic atoms. This highlights the tunability of magnetic properties in SiC nanotubes *via* group III element doping.

Table 8 shows the spin magnetic moments of individual atoms in single and double Ga-doped (6,0) SiC nanotubes, where Ga atoms substitute carbon sites. For the single Ga-doped system, one Ga atom replaces a carbon atom, resulting in a total magnetic moment of approximately $1.0\mu_B$. In this configuration, the spin polarization is primarily localized around the Ga dopant and its neighboring atoms. As shown in Table 8, carbon atom C18 exhibits a positive spin magnetic moment of approximately $0.219\mu_B$, contributing notably to the system's magnetization. Other nearby carbon atoms also display significant positive spin moments, including C8 ($0.250\mu_B$) and C12 ($0.250\mu_B$), which reinforce the local magnetic ordering induced by the Ga dopant. The Ga atom itself carries a substantial spin moment of $0.541\mu_B$, which is a major contributor to the net magnetic moment. In contrast, the surrounding silicon atoms generally show small negative spin moments, such as Si7 ($-0.144\mu_B$) and Si13 ($-0.121\mu_B$). These negative contributions partially offset the positive spin moments of carbon and Ga atoms but are not sufficient to cancel the overall spin polarization. As a result, the system maintains a net magnetic moment close to $1.0\mu_B$, indicating localized magnetic behavior.

In the double Ga-doped system, two Ga atoms replace two carbon atoms, significantly altering the magnetic landscape. Contrary to expectations of spin compensation, the total magnetic moment increases substantially to $6.0\mu_B$, suggesting strong spin polarization across the nanotube. Interestingly, in this configuration, the spin moments of the Ga atoms themselves are relatively small, with values of $0.041\mu_B$ and $0.039\mu_B$, indicating that their direct magnetic contribution is minimal. However, several carbon atoms now exhibit large positive spin moments. For instance, C4 and C16 each show a moment of $2.656\mu_B$, and C1 and C20 have moments of $1.986\mu_B$, highlighting an enhanced spin polarization effect propagated through the lattice by the presence of the two Ga atoms.

At the same time, many silicon atoms exhibit more pronounced negative spin moments than in the single-doped case, such as Si0 ($-0.715\mu_B$), Si3 ($-1.248\mu_B$), and Si7 ($-1.189\mu_B$). This reflects a more extensive antiferromagnetic interaction across the structure. Nonetheless, the significant positive contributions from carbon atoms dominate, leading to a net increase in the total magnetic moment.

In summary, single Ga doping leads to localized magnetic moments, primarily around the dopant site, resulting in a modest net magnetization of $1.0\mu_B$. On the other hand, double Ga doping does not lead to a compensated or neutral magnetic state; instead, it enhances spin polarization throughout the system, resulting in a much larger total magnetic moment of $6.0\mu_B$. This indicates that double Ga substitution at carbon sites in (6,0) SiC nanotubes promotes long-range magnetic interactions and overall ferromagnetic behavior.

Fig. 21 presents the spin-polarized DOS for a $SiC_{1-x}Ga_x$ nanotube system, where three silicon atoms are chemically bonded with a gallium (Ga) dopant. The DOS is split into spin-up and spin-down components, allowing analysis of the spin polarization induced by Ga doping. The Fermi level, marked by the vertical dashed blue line at 0 eV, serves as the reference point for electronic state occupation.

The asymmetry between the spin-up and spin-down DOS clearly indicates spin polarization in the system, suggesting a magnetic character induced by the substitutional Ga dopant. Near the Fermi level, there is a significant difference in the density of states for spin-up and spin-down electrons. This imbalance is a signature of spin splitting, commonly associated with localized magnetic moments and the breaking of spin degeneracy due to dopant-induced perturbations. Furthermore, the presence of states at or near the Fermi level in at least one of the spin channels suggests the system may exhibit metallic or half-metallic behavior. This is particularly relevant for potential

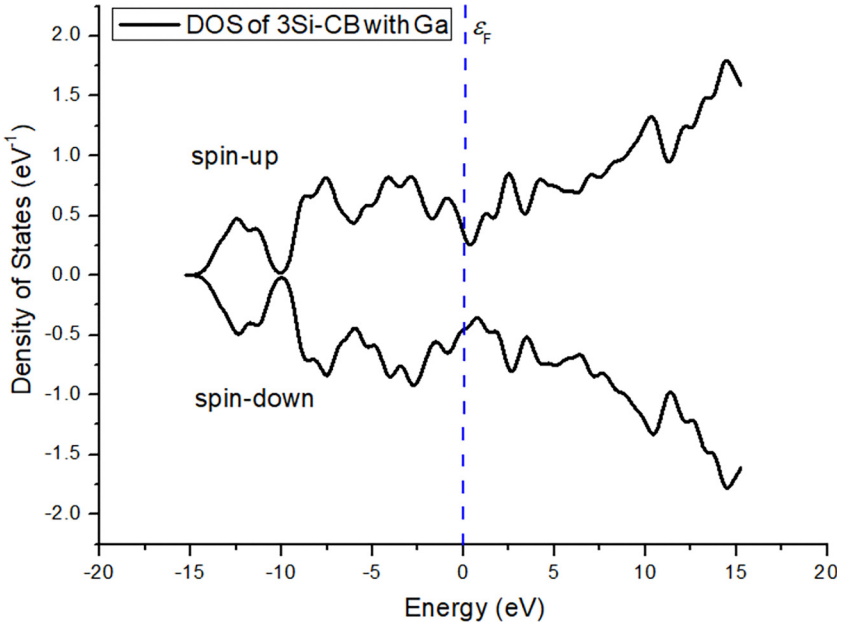

Fig. 21 Spin-polarization DOS diagrams for 3Si atoms chemically bonded (CB) with dopant in $SiC_{1-x}Ga_x$ NT.

applications in spintronic devices, where spin-polarized currents are desired.

Overall, the DOS analysis highlights the influence of Ga doping and specific Si–Ga chemical bonding on the electronic and magnetic properties of the SiC nanotube, potentially enabling tunable spintronic functionalities through controlled doping.

Fig. 22 demonstrates the spin-polarized charge density distribution when a Ga atom substitutes a carbon atom in the SWSiCNT. The isosurface plot shows the regions of electronic charge redistribution upon doping. The purple lobes around the Ga dopant and neighboring Si atoms indicate areas of electron accumulation, which arise due to charge transfer and reorganization of the electronic cloud. The cyan regions mark electron depletion, suggesting a local reduction in electron density compared to the pristine system. This redistribution reflects the interaction between the Ga dopant and the SiC lattice, indicating a modified bonding environment. The figure reveals that Ga at the C site significantly perturbs the local electronic structure, which can influence both the electronic and magnetic properties of the nanotube.

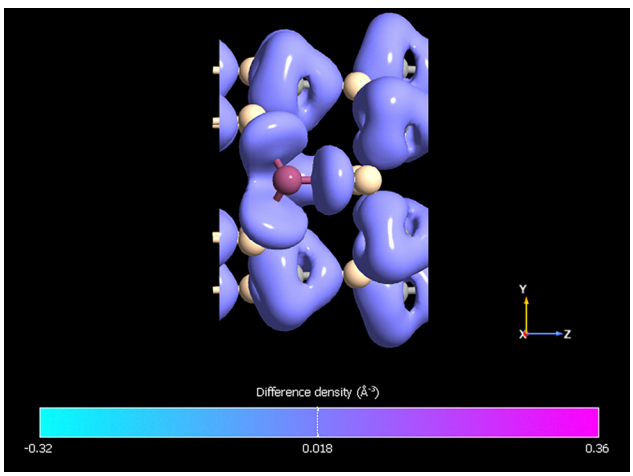

Fig. 22 Spin density isosurface plot for Ga doped at the C site in SWSiCNT. Purple regions represent charge accumulation, and cyan regions represent charge depletion. Beige, gray, and pink spheres correspond to Si, C, and Ga atoms, respectively.

For the Ga-doped (6,0) SWSiCNT system with substitution at the carbon site, the total energies of the FM and AFM states are found to be −4156.04843 eV and −4156.02891 eV, respectively. In this case, the energy difference is negative, showing that the FM configuration is energetically more stable than the AFM one. This result indicates a ferromagnetic ground state for the Ga(C)-doped SWSiCNT. The emergence of ferromagnetism due to Ga doping highlights its potential in magnetic and spintronic applications at the nanoscale.

Table 9 summarizes the total energy calculations for FM and AFM spin configurations in (6,0) SWSiCNTs doped with Al and Ga atoms at both Si and C lattice sites. For Al and Ga doping at the Si site, the AFM configuration is energetically more favorable, as indicated by positive ΔE values. In contrast, when Ga is substituted at the C site, the FM state becomes more stable (negative ΔE), suggesting that the magnetic ground state depends not only on the dopant type but also on its substitutional site. These results highlight the tunability of magnetic ordering in doped SWSiCNTs, which is of potential interest for nanoscale spintronic device applications.

Fig. 23 represents the comparative bar chart illustrating the magnetic ground states of doped (6,0) SWSiCNTs. The *y*-axis distinguishes ferromagnetic (FM) stable states (bars extending upward, blue) from antiferromagnetic (AFM) stable states (bars

Table 9 Total energies of FM and AFM configurations for Al- and Ga-doped (6,0) SWSiCNTs, with substitution at both Si and C sites

System	Doping site	E_{FM} (eV)	E_{AFM} (eV)	$\Delta E = E_{FM} - E_{AFM}$, (eV)	Preferred magnetic state
SWSiC:AlNT	Si	−3891.47261	−3912.51781	21.04520	AFM
SWSiC:GaNT	Si	−4108.82776	−4108.92690	0.09914	AFM
SWSiC:AlNT	C	−3956.66549	−3956.67554	0.01005	AFM
SWSiC:GaNT	C	−4156.04843	−4156.02891	−0.01952	FM

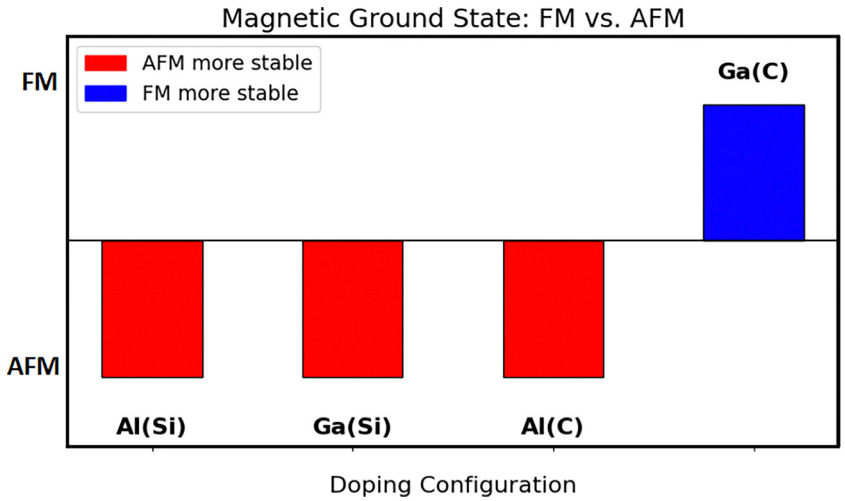

Fig. 23 Comparative bar chart illustrating the magnetic ground states of doped (6,0) SWSiCNTs.

extending downward, red). The doping configurations are labeled on the x-axis. The plot clearly shows that Al- and Ga-doping at the Si and C sites prefer AFM configurations, while Ga doping at the C site stabilizes the FM configuration.

As shown from Fig. 23, doping with Al and Ga atoms at the Si and C sites stabilizes the AFM ground state of the nanotube. In contrast, Ga doping at the C site favors the FM configuration. These results indicate that both the dopant element and its substitution site significantly influence the magnetic properties of the nanotube, providing valuable insights for the design of spintronic devices.

3.9. Stability of Al- and Ga-doped SWSiCNT systems at Si sites

To investigate the thermodynamic, mechanical, and kinetic stability of the Al- and Ga-doped SWSiCNT systems, we performed simulations using geometry-optimized structures within the framework of first-principles DFT. The total energy, atomic forces, and stress tensor were calculated to assess the stability and structural integrity of the doped nanotubes. These parameters are essential from a theoretical standpoint, as they offer a fundamental understanding of the energetic and structural behavior of the doped systems under equilibrium conditions and in response to external perturbations. The use of optimized geometries ensures that all evaluated properties correspond to the most stable atomic configurations, thus providing reliable insights into the intrinsic properties of these materials.

The total energy of a system is a central quantity in solid-state physics and quantum chemistry, reflecting the overall stability of a given atomic configuration. By comparing the total energy of doped and pristine systems, one can determine the thermodynamic stability, such as through formation energy calculations. A lower total energy indicates a more stable configuration, and negative formation energy typically suggests a thermodynamically favorable doping process.

The atomic forces, derived as the gradient of the total energy with respect to atomic positions, are essential for evaluating kinetic stability. In a fully relaxed and kinetically stable structure, the residual forces on each atom should approach zero, implying the system resides in a local minimum on the potential energy surface. Large residual forces would indicate that the structure is either not yet optimized or unstable and prone to structural rearrangement or distortion.

The stress tensor provides information on the internal mechanical state of the system. For a mechanically stable system under equilibrium conditions, the stress components (especially the diagonal terms representing pressure in the x, y, and z directions) should be close to zero. Significant residual stress suggests internal strain, which could compromise structural integrity or signal the need for further relaxation. This is particularly important for one-dimensional systems like nanotubes, where curvature, doping-induced strain, or axial deformation can strongly influence mechanical behavior.

Together, these parameters offer a comprehensive framework for assessing whether the doped SiC NT systems are stable enough for experimental synthesis and functional use. Systems that are thermodynamically favorable, kinetically relaxed, and mechanically balanced are more likely to retain their structure

under practical conditions and may serve as promising candidates for spintronic or nanomagnetic applications.

To comprehensively assess the stability of the Al- and Ga-doped SWSiCNTs at both Si and C sites, we analyzed key parameters including total energy, atomic forces, and the stress tensor. These parameters provide insight into the thermodynamic, kinetic, and mechanical stability of the doped systems, which are critical for their potential applications in nanoelectronics and spintronics.

Both Al- and Ga-doped SWSiCNTs at Si sites exhibit strongly negative total free energies, with the Al-doped system at approximately −3948.02 eV and the Ga-doped system even lower at −4045.52 eV. Such negative total energies indicate that doping with either Al or Ga is thermodynamically favorable, promoting stable formation of these substitutional defects in the nanotube lattice. This energy minimization confirms the feasibility of doping from a thermodynamic standpoint.

The atomic forces serve as a direct measure of kinetic stability. For the Al-doped system at Si site, residual forces on atoms are relatively low (generally below 0.05 eV $Å^{-1}$), with a net force near zero, indicating that the system is close to a local minimum on the potential energy surface and thus kinetically stable. Conversely, the Ga-doped system at Si site shows significantly higher atomic forces, particularly on the Ga dopant and neighboring Si atoms, with forces reaching up to ∼1.42 eV $Å^{-1}$. The net force magnitude is also larger in the Ga system. These high forces suggest that the Ga-doped nanotube has not fully relaxed and requires further structural optimization to reach kinetic equilibrium. Without minimizing these forces, the system remains dynamically unstable, this may affect device performance.

Analysis of the stress tensors reveals that the Al-doped system at Si site has very small residual stresses on the order of 10^{-4} eV $Å^{-3}$, indicating near mechanical equilibrium. In contrast, the Ga-doped system at Si site shows higher residual stresses, including larger off-diagonal shear components and normal stresses along the axial direction. These stresses imply lattice distortions due to the larger atomic radius and electronic structure of Ga compared to Al. Mechanical relaxation beyond the current level is necessary to relieve this strain and stabilize the system mechanically.

Fig. 24 represents thermodynamic, kinetic, and mechanical stability comparison of Al- and Ga-doped SiC nanotube systems at Si sites: (a) thermodynamic stability is represented by the total energy, where a lower value indicates a more stable configuration; (b) kinetic stability is evaluated using both the maximum atomic force and the net force acting on the system; lower forces suggest better relaxation and structural stability; (c) mechanical stability is assessed *via* the norm of the stress tensor; smaller stress values indicate minimal internal pressure and better mechanical equilibrium. Overall, the Al-doped system, with Al atoms doped at Si sites, shows lower forces and stress, indicating superior structural and mechanical stability compared to the Ga-doped configuration, where Ga is also doped at Si sites. The optimized geometry results for atomic forces and stress tensors in SiC nanotubes with Al and Ga doped at Si sites are provided in SI4. These data further support the evaluation of kinetic and mechanical stability for the doped configurations.

In addition to geometry optimization, *ab initio* molecular dynamics (AIMD) simulations were conducted to assess the thermal stability of Al- and Ga-doped single-walled SiC nanotubes at Si sites. Monitoring total energy fluctuations over time provides insights into the system's response to thermal perturbations, confirming its structural robustness. This approach aligns with methodologies discussed in the literature, such as those by Lau *et al.*,[47] who reviewed the mechanical properties of carbon nanotube composites. Before conducting AIMD simulations, it was anticipated that both Al- and Ga-doped SiC nanotubes would exhibit thermal resilience, maintaining their structural framework without significant bond breakage or deformation under thermal agitation. Given the high covalent bonding nature of the SiC lattice and the chemical similarity of Al and Ga to Si, it was expected that substitution at Si sites would induce only localized distortions rather than global instability. Additionally, small oscillations in total

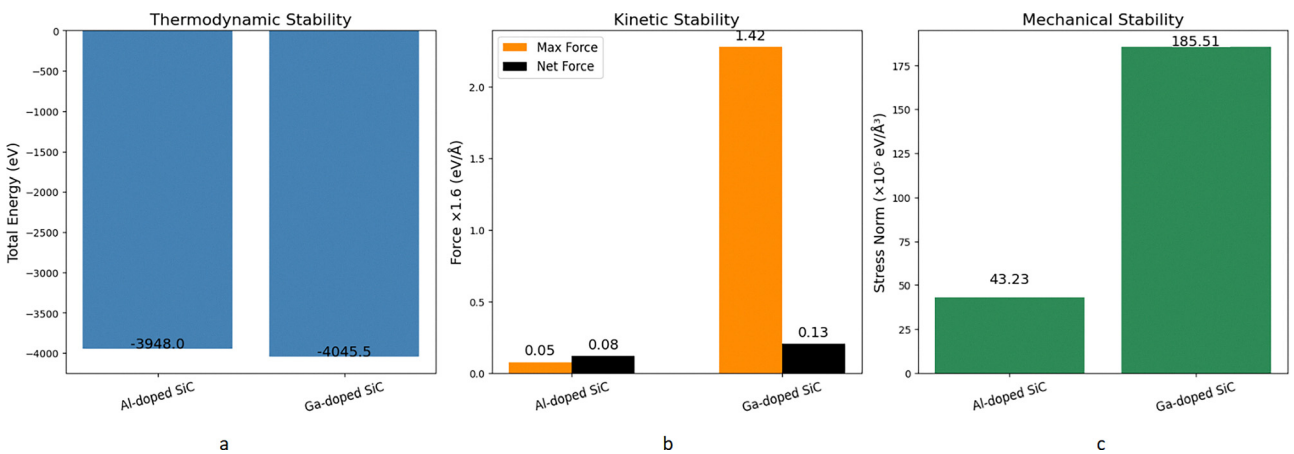

Fig. 24 Comparison of stability parameters for Al- and Ga-doped SiC nanotubes at Si sites: (a) total energy (thermodynamic stability), (b) net and maximum forces (kinetic stability), and (c) stress tensor norm (mechanical stability).

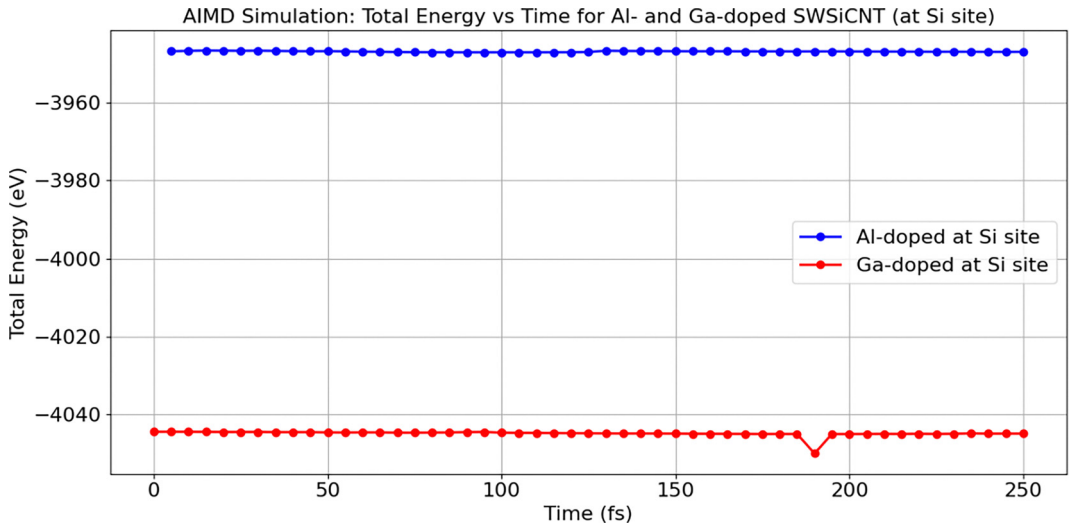

Fig. 25 Time evolution of total energy during the AIMD simulation of Al- and Ga-doped SWSiCNTs at Si sites.

energy around a mean value were anticipated, indicating the system had reached thermal equilibrium and was dynamically stable throughout the simulation period.

Fig. 25 demonstrates the total energy results over 0 to 250 fs (femtoseconds) from AIMD simulations of SWSiCNTs doped with Al and Ga at Si sites. The system exhibits minimal total energy fluctuations (less than or around 0.1 eV), indicating thermodynamic equilibrium and confirming the thermal stability of the doped structures.

Key observations from the AIMD data for Al-doped SWSiCNT at Si site include that the potential energy remains relatively stable throughout the simulation, fluctuating slightly around −3947.4 eV, which indicates that the aluminum-doped single-walled silicon carbide nanotube maintains structural stability during the AIMD simulation. The kinetic energy varies between approximately 0.34 eV and 0.81 eV, reflecting the atomic motion and corresponding thermal activity within the system. The total energy is consistently negative and stable, showing only minor fluctuations that correspond to the combined changes in potential and kinetic energies, demonstrating good energy conservation throughout the simulation. The instantaneous temperature fluctuates between roughly 116 K and 273 K, indicating normal thermal variations expected in molecular dynamics simulations under these conditions. From the AIMD simulations dates for Ga doping at the Si site reveal that the potential energy remains consistently stable around −4045 eV, indicating the structural integrity of the Ga-doped SWSiCNT throughout the simulation. The kinetic energy fluctuates between approximately 0.55 eV and 1.01 eV, which corresponds to the vibrational and thermal motion of atoms within the system. The total energy is consistently around −4044 eV, showing only slight variations, which confirms good energy conservation during the molecular dynamics run. The instantaneous temperature varies between about 199 K and 341 K, reflecting expected thermal fluctuations for the system under study. These results suggest that Ga doping at the Si site maintains the energetic and thermal stability of the nanotube and does not induce significant destabilization over the simulation timeframe. The total energy remains quite stable with small fluctuations (~0.1–0.2 eV), which is a good sign of system stability and no major structural disruptions due to Ga doping at the Si site. The temperature fluctuations are typical in MD simulations, but the downward trend towards the end might mean the system is losing some kinetic energy or cooling.

Overall, both Al and Ga doping at the silicon site preserve the energetic stability of the SWSiCNT over the simulation period. The Al-doped nanotube exhibits consistent energetic and thermal stability, indicating strong kinetic and mechanical robustness and suggesting it is well-relaxed for practical applications. In contrast, while the Ga-doped system is thermodynamically stable, it shows greater atomic fluctuations and requires further optimization to fully minimize atomic forces and stresses, ensuring comparable kinetic and mechanical stability. This comparison highlights that although both dopants are viable for SiC nanotubes from a thermodynamic perspective, a comprehensive assessment of kinetic and mechanical stability is essential for confirming their suitability in functional nanomaterial design.

The AIMD calculation results for forces, stress, and total energy *versus* time for SiC NTs with Al- and Ga-doping at Si sites are provided in SI5.

3.10. Stability of Al- and Ga-doped SWSiCNT systems at C sites

To assess the stability of Al- and Ga-doped single-walled SiC nanotube (SWSiCNT) systems at carbon substitution sites, we conducted comprehensive geometry optimizations using density functional theory (DFT). The calculations provided total energies, atomic forces, and stress tensors, enabling evaluation of both the thermodynamic and mechanical stability of the doped structures. The results demonstrate that substitution of

carbon atoms with Al or Ga yields locally stable configurations, confirming that such doping is energetically favorable and structurally feasible under equilibrium conditions.

In addition to static geometry optimizations, *ab initio* molecular dynamics (AIMD) simulations were carried out to probe the thermal stability of these doped nanotubes. By monitoring the time evolution of total energy and atomic positions at finite temperatures, AIMD simulations provide insights into the system's response to thermal fluctuations. The relatively small energy fluctuations and preserved structural integrity throughout the simulation period corroborate the robustness of Al- and Ga-doped SWSiCNTs under thermal stress, underscoring their potential applicability in high-temperature environments. This methodology is consistent with approaches found in the literature, for instance, the study by Lau *et al.*,[47] which examined the mechanical characteristics of carbon nanotube/polymer composites.

The optimized geometry calculations yield total energies of −3970.03093 eV for the Al-doped SWSiCNT system and −4069.52124 eV for the Ga-doped system at carbon substitution sites. The lower total energy observed for the Ga-doped structure suggests a slightly more energetically favorable configuration compared to the Al-doped counterpart. Both systems exhibit significantly negative total energies, indicating stable, bound states following doping. These results reinforce the conclusion that substitution of carbon atoms by either Al or Ga leads to thermodynamically stable configurations within the nanotube framework.

The forces acting on the atoms in the optimized structures of Al- and Ga-doped SWSiCNTs are generally low, indicating that the geometries are close to equilibrium configurations. For the Al-doped system, the maximum atomic force magnitude observed is approximately 0.0493 eV Å^{-1}, with a net force on the system of about 0.13 eV Å^{-1} along the *z*-axis. Similarly, the Ga-doped structure exhibits slightly higher maximum atomic forces, reaching up to 0.0446 eV Å^{-1} on the Ga atom itself, and a net force magnitude around 0.15 eV Å^{-1}. These small residual forces suggest that the geometry optimizations converged satisfactorily, and the structures are mechanically stable.

The computed stress tensors for both doped systems show minimal anisotropy and low magnitudes on the order of 10^{-4} eV Å^{-3}, with slight compressive and tensile components balanced across different directions. For the Al-doped nanotube, the diagonal components range from approximately -5.3×10^{-4} to 5.4×10^{-4} eV Å^{-3}, while the Ga-doped system shows similar values in the range of -6.2×10^{-4} to 3.8×10^{-4} eV Å^{-3}. These small stress values confirm that the doped nanotube lattices are mechanically relaxed and free of significant residual strain.

Fig. 26 shows a comparison of stability parameters for Al- and Ga-doped SiC nanotubes at carbon substitution sites. Panel (a) illustrates the thermodynamic stability in terms of total energy, where the Ga-doped system exhibits a slightly lower total energy (−4069.52 eV) than the Al-doped counterpart (−3970.03 eV), suggesting that Ga doping is marginally more energetically favorable. Panel (b) presents the kinetic stability by showing the maximum and net atomic forces. The maximum force is slightly higher in the Al-doped system (0.049 eV Å^{-1}) compared to the Ga-doped system (0.045 eV Å^{-1}), whereas the Ga-doped system has a slightly higher net force (0.15 eV Å^{-1}) than the Al-doped case (0.13 eV Å^{-1}), indicating that both configurations are kinetically stable with minor variations. Panel (c) displays the mechanical stability using the stress tensor norm, where both systems demonstrate low stress values 0.00080 eV Å^{-3} for Al and 0.00078 eV Å^{-3} for Ga confirming that both doped structures are mechanically stable. Collectively, the results indicate that Al and Ga substitutions at carbon sites in SiC nanotubes yield structurally and thermodynamically stable systems, with Ga doping providing a slight energetic advantage.

The optimized geometry results for atomic forces and stress tensors in SWSiCNTs with Al and Ga doped at C sites are provided in SI4.

The first-principles results from AIMD simulations of the total energy evolution over time for a SWSiCNT doped with Al atoms substituting C sites track key thermodynamic quantities

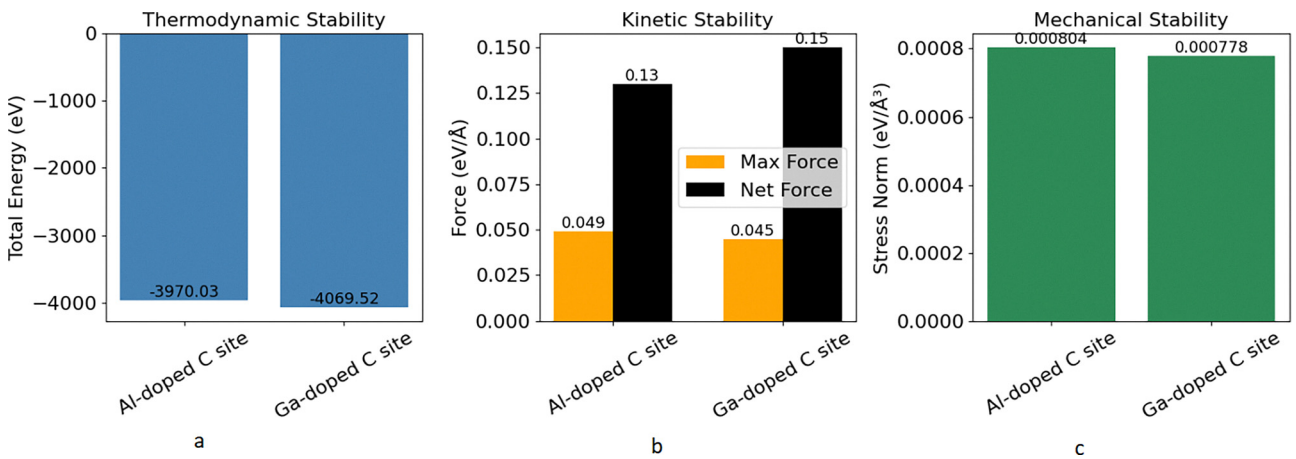

Fig. 26 Comparison of stability parameters for Al- and Ga-doped SiC nanotubes at C sites: (a) total energy (thermodynamic stability), (b) net and maximum forces (kinetic stability), and (c) stress tensor norm (mechanical stability).

including potential energy, kinetic energy, total energy, and instantaneous temperature during the simulation time steps ranging from 0 to 250 fs. At the initial time step (0 fs), the system starts in equilibrium at room temperature (300 K), reflected by low kinetic energy and a corresponding potential energy value. As the simulation precedes, the kinetic energy and thus the instantaneous temperature increases, indicating increased atomic vibrations and thermal excitation within the nanotube structure.

From 0 to approximately 50 fs, the temperature rises sharply from 300 K to over 1300 K, showing the system's initial heating phase. During this period, the potential energy decreases slightly, suggesting structural relaxation and stabilization as the aluminum dopant interacts with the carbon lattice. Between 50 and 160 fs, the system reaches a thermal peak with instantaneous temperatures exceeding 1700 K. The potential energy remains fairly stable and negative, indicating that the overall structural integrity is maintained despite the elevated thermal conditions. The total energy shows minimal fluctuations throughout, demonstrating good energy conservation and numerical stability of the AIMD simulations. Following this peak, the temperature and kinetic energy fluctuate within a narrower range, between approximately 1400 K and 1800 K, signifying that the system achieves a dynamic thermal equilibrium. This balance implies stable atomic vibrations without any significant structural degradation.

Our AIMD results for Ga doping at the C site in SWSiCNTs demonstrate how the system's energy and temperature evolve over the simulation time. The data include the simulation step, time (in femtoseconds), potential energy, kinetic energy, total energy, and instantaneous temperature derived from the kinetic energy. The energies reflect the dynamic behavior of the system, showing variations in atomic interactions and movement. The total energy remains relatively stable, indicating a well-conserved simulation, while the temperature changes correspond to the thermal fluctuations within the nanotube structure during the AIMD run. The system starts at a temperature of 300 K (room temperature). As the simulation progresses, both kinetic energy and instantaneous temperature generally increase, indicating heating of the system. This rise corresponds to energy fluctuations as the atoms move and the system reaches thermal equilibrium.

Throughout the simulation, the potential energy fluctuates slightly but stays around a consistent negative value, reflecting the stable bonding environment within the Ga-doped nanotube. The kinetic energy increases over time in the early steps, indicating growing atomic motion and energy distribution among the atoms. The total energy remains relatively stable around −4063 eV, showing good energy conservation in the simulation and indicating numerical stability. Minor fluctuations in potential and kinetic energies are typical in AIMD simulations due to atomic vibrations and thermal motion. The instantaneous temperature rises initially, reaching above 1500 K at certain points, which suggests increased atomic vibrations due to thermal excitation. After peaking, the temperature shows some fluctuations but generally remains elevated, illustrating how doping affects the thermal behavior of the silicon carbon nanotube. These temperature and energy trends provide insights into the structural dynamics and thermal stability of the Ga-doped system during the simulation time frame.

Fig. 27 presents the variation of total energy as a function of simulation time for SWSiCNTs doped with Al and Ga at the C site, based on AIMD simulations. The time evolution of total energy provides insights into the thermodynamic stability of the doped systems under thermal excitation. As shown in the plot: both systems exhibit fluctuations in total energy, characteristic of thermal vibrations during the simulation. The Al-doped SWSiCNT (blue line) maintains a relatively stable total energy around −3961.8 eV, with minor fluctuations throughout the 250 fs simulation. The Ga-doped SWSiCNT (red line) also shows energy oscillations, but it consistently maintains a more

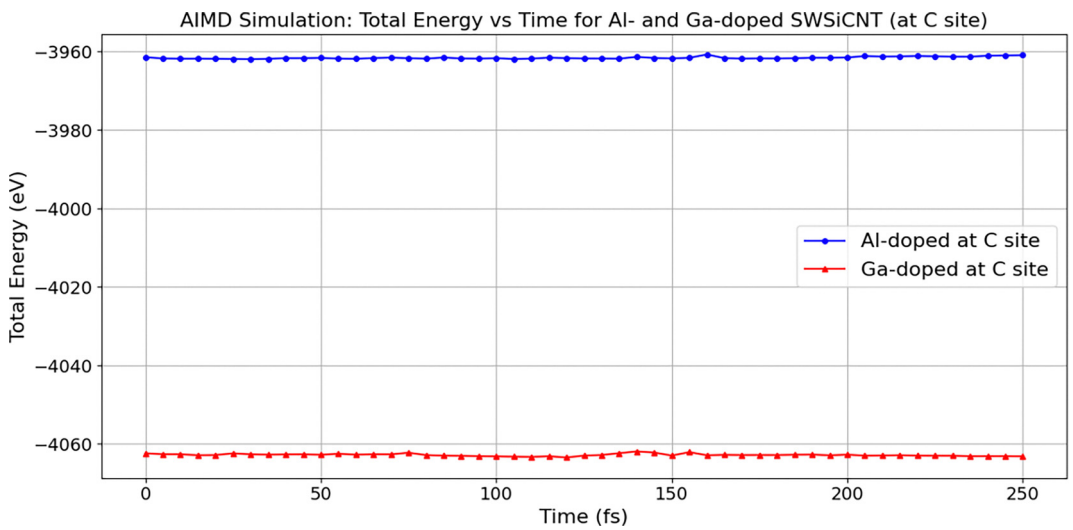

Fig. 27 Time evolution of total energy during the AIMD simulation of Al- and Ga-doped SWSiCNTs at C sites.

negative total energy near −4063.0 eV, indicating a more energetically favorable or thermodynamically stable configuration under the same conditions. These results suggest that Ga substitution at the C site may provide a slightly more stable structural configuration compared to Al substitution, at least in terms of total energy. However, other factors such as structural distortions, electronic properties, and temperature effects should also be considered for a complete assessment.

Overall, these results confirm that Al doping at the carbon site in SWSiCNT maintains structural stability under high-temperature conditions, which is promising for applications requiring thermal resilience in nanoscale devices. The low forces and negligible stresses in both Al- and Ga-doped SWSiCNTs indicate that substitutional doping at carbon sites yields mechanically relaxed configurations, consistent with the total energy results.

The AIMD calculation results for forces, stress, and total energy *versus* time from 0 to 250 fs for SWSiCNTs with Al- and Ga-doping at C sites are provided in SI5.

3.11. Formation energy of single and double Al/Ga doped (6,0) SWSiCNTs at Si/C sites

In nanoscale materials, the formation of defects and dopants plays a critical role in determining their physical and chemical properties. Understanding the formation energy of these defect structures is essential, as it quantifies the energetic cost associated with incorporating dopants into the host lattice. This parameter not only reflects the thermodynamic stability of the doped system but also directly influences the feasibility of synthesis and fabrication processes.

In practical terms, formation energy affects how easily dopants can be introduced and maintained within the nanotube structure during material growth or device manufacturing. Lower formation energies typically indicate more stable and experimentally achievable doping configurations, which is vital for designing reliable nanoscale devices, including spintronic and magnetic applications. Conversely, high formation energies suggest that the doped structure may be difficult to realize or maintain, limiting its practical applicability.

In this study, we calculated the formation energies of both single and double Al- and Ga-doped (6,0) SWSiCNTs at substitutional Si and C sites to evaluate their relative stability and potential for experimental realization.

The formation energy E_f was calculated using the following expression:

$$E_f = E_{doped} - E_{pristine} - n\cdot\mu_{Al/Ga} + n\cdot\mu_{Si/C} \quad (5)$$

where E_{doped} and $E_{pristine}$ are the total energies of the doped and pristine nanotubes, respectively; $\mu_{Al/Ga}$ and $\mu_{Si/C}$ represent the chemical potentials of the dopant and substituted atoms; and n is the number of dopants (1 for single doping and 2 for double doping).

In the presented work, the chemical potential values for Al, Ga, Si, and C atoms were taken as −2.269118 eV (Al), −2.228112 eV (Ga), −3.686924 eV (Si), and −5.114380 eV (C), respectively, and using these values, the defect formation energy was calculated. The value of $E_{pristine}$ = −3983.35741 eV, obtained from our calculations, was used in the formation energy calculations and is reported in Table 10. Table 10 summarizes the calculated formation energies for all single and double doping configurations at both Si and C sites.

Table 10 Calculated total energies (E_{doped}) and formation energies (E_f) for single and double doping of Al and Ga atoms at Si and C sites in SiC nanotubes. The dopant concentration *xxx* is given in percentage (%)

System	*x*, %	E_{doped}, eV	E_f, eV
$Si_{11}Al_1C_{12}$	8.3	−3948.01546	33.92414
$Si_{10}Al_2C_{12}$	16.6	−3891.47261	89.04919
$Si_{11}Ga_1C_{12}$	8.3	−4046.11780	−64.21920
$Si_{10}Ga_2C_{12}$	16.6	−4108.82776	−128.3887
$Si_{12}C_{11}Al_1$	8.3	−3970.03093	10.48122
$Si_{12}C_{10}Al_2$	16.6	−3960.21974	17.44715
$Si_{12}C_{11}Ga_1$	8.3	−4069.52124	−89.05010
$Si_{12}C_{10}Ga_2$	16.6	−4156.04843	−178.46356

The results indicate that Ga doping at both Si and C sites consistently yields negative formation energies, suggesting that Ga incorporation is energetically favorable and likely to produce stable defect structures within the SiC nanotubes. Al doping, on the other hand, shows positive formation energies for both Si and C sites, suggesting that Al substitution is less energetically favorable and the formation of such defects may require additional energy input. Formation energies increase with higher dopant concentrations (double doping) for Al, meaning it becomes even less favorable as the doping level rises. Conversely, Ga shows a trend of increasingly negative formation energies with double doping, suggesting that higher Ga doping concentrations are thermodynamically preferred.

These findings complement our magnetic ground state analysis and offer comprehensive insights into the energetic favorability and synthesis feasibility of various doped SWSiCNTs. Understanding these formation energies is crucial for guiding experimental efforts and optimizing the design of nanotube-based devices for spintronics and other advanced nanotechnological applications. The calculations reveal that Ga is a more suitable dopant for SiC nanotubes compared to Al, both in terms of energetic favorability and doping site preference. Ga doping stabilizes the nanotube structure more effectively at both Si and C substitutional sites. This aligns with previous observations of Ga's ability to integrate well within semiconductor lattices due to its chemical and electronic properties. This analysis provides valuable insight into the design and optimization of doped SiC nanotubes for applications requiring specific electronic or mechanical characteristics. Future experimental and theoretical studies can build upon these results to explore the practical implications of Ga doping in nanodevices.

3.12. Phonon band structure analysis for Al- and Ga-doped SWSiCNT

Phonon band structure analysis provides a fundamental understanding of the dynamical stability and lattice vibrational properties of doped SiCNT systems. The phonon spectra of

the Al- and Ga-doped single-walled SiCNTs were computed for both silicon and carbon substitutional sites using the finite-displacement method within the LSDA framework. The resulting dispersion curves, presented in Fig. 28, confirm that all four doped configurations are dynamically stable, as evidenced by the absence of imaginary (negative) frequencies throughout the Brillouin zone. This demonstrates that both Al and Ga dopants can be successfully incorporated into the SiCNT lattice without inducing lattice instabilities or phonon softening that could compromise structural integrity.

The phonon dispersion of the Al-doped SiCNT at the silicon site shows no imaginary frequencies and a well-defined distribution of acoustic and optical branches. The three acoustic modes near the Γ point smoothly approach zero, confirming translational invariance and mechanical stability. The optical branches extend up to approximately 125 meV, indicating strong Si–C and Al–C bond stiffness in the local environment. A slight upward shift of high-frequency optical modes compared with the pristine nanotube suggests phonon hardening due to local charge redistribution and stronger bonding near the Al dopant. This behavior reflects enhanced rigidity of the lattice in the vicinity of the substitutional Al atom.

For the configuration where Al substitutes a carbon atom, the overall phonon profile remains stable without any negative frequencies. However, the low-frequency acoustic modes below 20 meV exhibit minor flattening compared with the Si-site case, indicating softening associated with mass and bond-length mismatch between Al and the neighboring Si atoms. This local softening corresponds to weak lattice relaxation but does not induce any instability, as all branches remain positive across the Γ–Z path. The high-frequency optical region (100–120 meV) remains nearly unchanged, demonstrating that Al doping at the C site preserves the vibrational integrity of the SiC nanotube framework.

In the Ga-doped SiCNT where substitution occurs at the Si site, the phonon spectrum also exhibits complete stability with no imaginary modes. Compared with Al doping, the Ga-doped system presents slightly lower optical frequencies ($\sim$115 meV), which can be attributed to the heavier atomic mass of Ga and its relatively weaker Ga–C bond strength compared with Al–C. The acoustic branches show a steeper dispersion near the Γ point, implying stronger lattice coupling along the nanotube axis. The overall behavior indicates that Ga incorporation at the Si site induces phonon softening in high-energy optical modes, yet maintains complete dynamical stability.

For Ga doping at the carbon site, the phonon spectrum remains free of imaginary frequencies, confirming the stability of this configuration as well. The low-frequency acoustic region

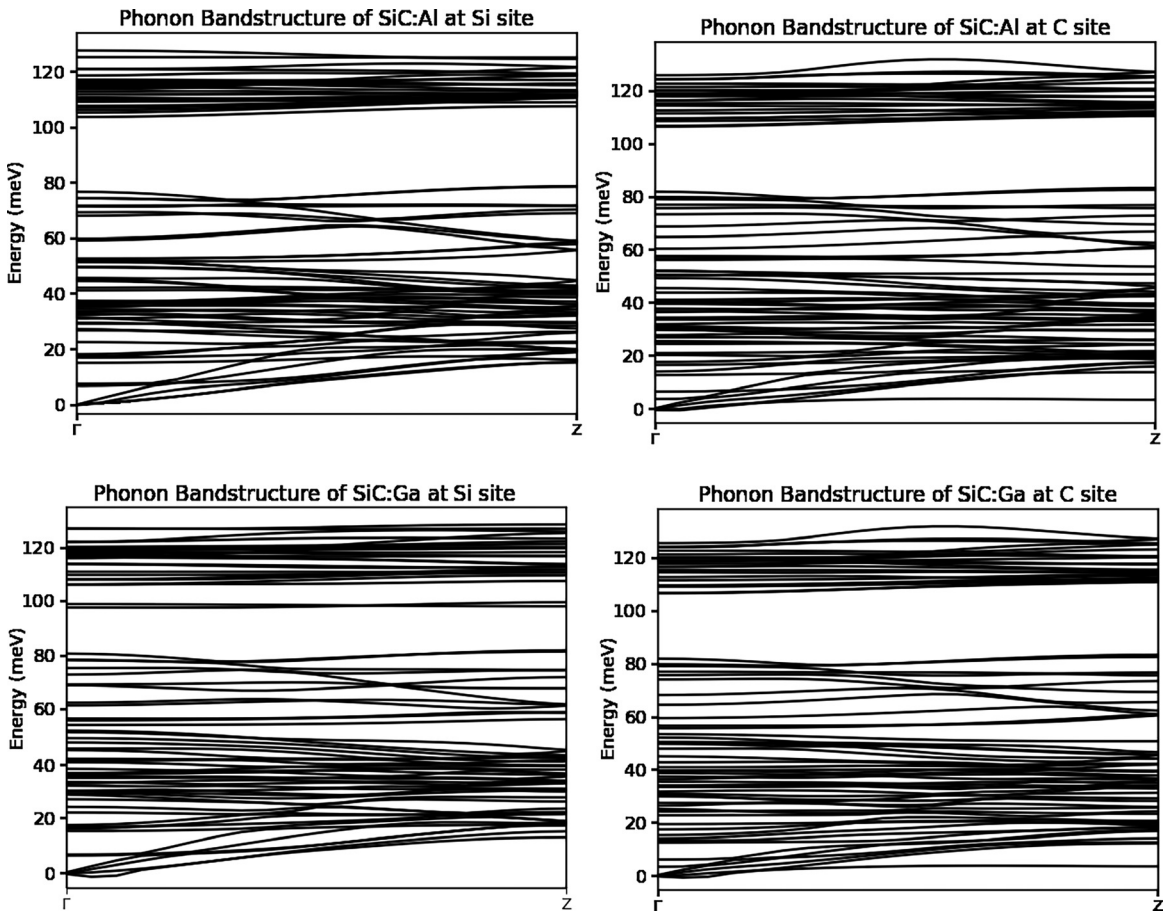

Fig. 28 Phonon band structures of Al- and Ga-doped (6,0) SWSiCNTs at Si and C sites.

exhibits slightly more pronounced flattening than in the Al-doped C-site case, consistent with local strain relaxation around the heavier Ga atom. Despite this, the optical modes extend up to ~120 meV, and the separation between acoustic and optical branches remains distinct. This behavior signifies that Ga substitution at the C site introduces localized mass-induced softening but does not compromise the lattice dynamical integrity. The maintained positive curvature of the acoustic branches indicates good mechanical resilience and phonon transport continuity along the nanotube axis.

4. Conclusion

We carried out a comprehensive first-principles study of the electronic, magnetic, and structural properties of Al- and Ga-doped single-walled (6,0) SiC nanotubes (SWSiCNTs) using density functional theory. Our findings demonstrate that doping with Al or Ga at Si or C sites enables precise control over the nanotubes' behavior. When Al is substituted at a Si site, the system becomes half-metallic at 8.3% doping (spin-up gap ~1.40 eV; spin-down channel metallic), and at 16.6% both spin channels become metallic. Ga doping at Si sites shows semiconducting gaps at lower concentration (≈1.0 eV for spin-up, ≈0.6 eV for spin-down), turning half-metallic at higher concentration. Doping at carbon sites preserves semiconducting behavior in both spins but introduces strong spin asymmetry: for example, Al-at-C yields gaps of ~0.66 eV (spin-up)/~0.51 eV (spin-down) at 8.3%, narrowing to ~0.60 eV/~0.12 eV at 16.6%; Ga-at-C gives ~0.44 eV/~0.60 eV at lower doping, with both gaps reducing to ~0.26 eV at higher concentration.

Magnetic moment calculations reveal that single dopants produce ~1.0μ_B each, largely localized on the carbon atoms bonded to the dopant. For double doping at C sites, Al yields a much larger total moment (~8.49μ_B), and Ga gives ~6.00μ_B. Dopant atoms (Al/Ga) and neighboring Si atoms often carry negative spin moments, indicating AFM coupling with adjacent carbon atoms. Analysis of magnetic ground states shows dopants at Si sites favor antiferromagnetic ordering, while Ga substitution at the C site leads to a FM ground state.

On structural stability, formation energies show that Ga doping (both at Si and C sites) is energetically more favorable (negative formation energies), whereas Al substitution has positive formation energies that grow larger with increasing doping level. Kinetic and mechanical stability assessments show that Al-doped nanotubes, especially for substitution at Si sites, have lowers residual atomic forces and stress tensor norms. Although Ga-doped structures are thermodynamically stable, they exhibit higher residual forces and stresses, indicating that further structural relaxation may be required. *Ab initio* molecular dynamics over ~250 fs confirms that both doped systems maintain integrity under thermal fluctuation: total energy fluctuations are small (~0.1–0.2 eV), with no bond breakage or major deformation. On the other hand, the absence of imaginary phonon modes in the calculated phonon band structures demonstrate that both Al- and Ga-doped SiCNTs at Si and C sites are dynamically stable, ensuring the reliability of their predicted electronic and magnetic properties for practical applications.

Altogether, our study confirms that by selecting dopant type (Al *vs.* Ga), doping site (Si *vs.* C), and dopant concentration, one can finely tune the electronic structure (from semiconducting to half-metallic to metallic), the magnitude and distribution of magnetic moments, and the mechanical robustness of SiC nanotubes. Ga-doping at C sites emerges as particularly favorable in terms of energetics, while Al-doping tends to deliver better mechanical stability. These insights position Al- and Ga-doped (6,0) SWSiCNTs as highly promising for spintronic applications and nanoelectronic devices, where engineered spin-dependent conduction and thermal/mechanical reliability are crucial.

Author contributions

The manuscript was written through contributions of all authors.

Conflicts of interest

There are no conflicts to declare.

Data availability

The data supporting this article have been included as part of the Supplementary information (SI). Supplementary information: supplementary dates and figures. See DOI: **https://doi.org/10.1039/d5cp03523f**.

References

1 W. Zhang, F. Zhang, Z. Zhang, S. Lu and Y. Yang, *Sci. China, Phys. Mech.*, 2010, **53**, 1582–1589.
2 R. Madar, *Nature*, 2004, **430**, 974–975.
3 A. Gali, *Phys. Rev. B: Condens. Matter Mater. Phys.*, 2006, **73**, 245415.
4 K. M. Alam and A. K. Ray, *Phys. Rev. B: Condens. Matter Mater. Phys.*, 2008, **77**, 035436.
5 B. Baumeier, P. Krüger and J. Pollmann, *Phys. Rev. B: Condens. Matter Mater. Phys.*, 2007, **76**, 085407.
6 S. Mukherjee and A. K. Ray, *J. Comput. Theor. Nanosci.*, 2008, **5**, 1210–1219.
7 J. S. Ponraj, S. C. Dhanabalan, G. Attolini and G. Salviati, *Crit. Rev. Solid State Mater. Sci.*, 2016, **41**, 430–446.
8 R. Yakimova, R. M. Petoral Jr., G. R. Yazdi, C. Vahlberg, A. L. Spetz and K. Uvdal, *J. Phys. D: Appl. Phys.*, 2007, **40**, 6435–6442.
9 M. A. Mahdy, S. H. Kenawy, E. M. A. Hamzawy, G. T. El-Bassyouni and I. K. El Zawawi, *Ceram. Int.*, 2021, **47**, 12047–12055.
10 M. L. Sun, Q. Q. Ren, Y. M. Zhao, J. P. Chou, J. Yu and W. C. Tang, *Carbon*, 2017, **120**, 265–273.

11 E. Santos, A. Ayuela and D. Sanchez-Portal, *New J. Phys.*, 2010, **12**, 053012.
12 J. X. Zhao and Y. H. Ding, *J. Phys. Chem. C*, 2008, **112**, 2558–2564.
13 H. Heidarzadeh, *Opt. Quant. Electron.*, 2019, **51**, 32.
14 A. T. Mulatu, K. N. Nigussa and L. D. Deja, *Opt. Mater.*, 2022, **134**, 113094.
15 Ch Vatankhah and H. A. Badehian, *Optik*, 2021, **237**, 166740.
16 W. Wang, J. Xu, Y. Zhang and G. Li, *Comput. Chem.*, 2017, **5**, 159–171.
17 M. N. Huda and A. K. Ray, *Chem. Phys. Lett.*, 2008, **457**, 124–129.
18 R. Z. Ibaeva, V. N. Jafarova, V. I. Eminova, I. C. Scurtu and S. Lupu, *J. Nanopart. Res.*, 2024, **26**, 23.
19 V. N. Jafarova, S. S. Rzayeva, I. C. Scurtu, C. Stanca, N. Acomi and G. Raicu, *Adv. Nat. Sci.: Nanosci. Nanotechnol.*, 2024, **15**, 035012.
20 V. N. Jafarova, V. I. Eminova, M. A. Musaev and I. C. Scurtu, *Technium*, 2025, **26**, 1–8.
21 N. T. Tien, P. T. B. Thao, V. N. Jafarova and D. Dey Roy, *Silicon*, 2024, 1–19.
22 S. Rzayeva, V. N. Jafarova and D. Dey Roy, *Mater. Sci. Semicond. Process.*, 2025, **197**, 109702.
23 S. Rzayeva and V. N. Jafarova, *Turk. Comput. Theor. Chem.*, 2025, **9**, 112–120.
24 S. Rzayeva and V. N. Jafarova, *J. Polytech.*, 2025, **28**, 947–955.
25 A. Q. Wu, Q. G. Song and L. Yang, *Adv. Mater. Res.*, 2012, **510**, 747–752.
26 A. A. Peyghan, A. Soltani, A. A. Pahlevani, Y. Kanani and S. Khajeh, *Appl. Surf. Sci.*, 2013, **270**, 25–32.
27 M. D. Mohammadi, H. Y. Abdullah, G. Biskos and S. Bhowmick, *C. R. Chim*, 2021, **24**, 291–304.
28 H. Tavakol and H. Haghshenas, *Quantum Rep.*, 2021, **3**, 366–375.
29 S. S. Hardisty, X. Lin, A. R. J. Kucernak and D. Zitoun, *Carbon Energy*, 2023, **6**, e409.
30 D. Wang, Z. Yuan, X. Wu, W. Xiong, J. Ding, Z. Zhang and W. Huang, *ACS Catal.*, 2023, **13**, 7132–7138.
31 J. Wu, H. Shi, K. Li and X. Guo, *Curr. Opin. Chem. Eng.*, 2023, **40**, 100923.
32 M. Ramadoss, H. Yu, A. Rajkamal, G. J. Yun, Z. Zhang, C. Yang, F. Ma, Y. Wu, C. Daiqian and Y. Chen, *J. Mater. Chem. A*, 2024, **12**, 30798–30809.
33 Y. S. Itas, R. Razali, S. Tata, A. M. Idris and M. U. Khandaker, *J. Energy Storage*, 2023, **72**, 108534.
34 F. Yang, S. Ghatak, A. A. Taskin, K. Segawa, Y. Ando, M. Shiraishi, Y. Kanai, K. Matsumoto and A. Rosch, *Phys. Rev. B*, 2016, **94**, 075304.
35 W. Liu, Q. Li, X. Yang, X. Chen and X. Xu, *Catalysts*, 2020, **10**, 769.
36 W. Kohn and L. J. Sham, *Phys. Rev.*, 1965, **140A**, 1133–1138.
37 V. N. Jafarova, *Pramana – J. Phys.*, 2024, **98**, 82–93.
38 M. Fuchs and M. Scheffler, *Comput. Phys. Commun.*, 1999, **119**, 67–98.
39 M. Cococcioni and S. de Gironcoli, *Phys. Rev. B: Condens. Matter Mater. Phys.*, 2005, **71**, 035105.
40 S. L. Dudarev, G. A. Botton, S. Y. Savrasov, C. J. Humphreys and A. P. Sutton, *Phys. Rev. B: Condens. Matter Mater. Phys.*, 1998, **57**, 1505.
41 A. I. Liechtenstein, V. I. Anisimov and J. Zaanen, *Phys. Rev. B: Condens. Matter Mater. Phys.*, 1995, **52**, R5467.
42 S. C. North, K. R. Jorgensen, J. Pricetolstoy and A. K. Wilson, *Front. Chem.*, 2023, **11**, 1152500.
43 W. Gough, *J. Phys. A: Gen. Phys.*, 1968, **1**, 704.
44 H. J. Monkhorst and J. D. Pack, *Phys. Rev. B: Condens. Matter Mater. Phys.*, 1976, **13**, 5188–5192.
45 ed. G. L. Harris, *Properties of Silicon Carbide*, INSPEC, Institution of Electrical Engineers, London, 1995.
46 G. L. Zhao and D. Bagayoko, *New J. Phys.*, 2000, **2**, 16.
47 K.-T. Lau, C. Gu and D. Hui, *Compos. Part B: Eng.*, 2006, **37**, 425–436.

